Water Biology and Security 4 (2025) 100370

Contents lists available at ScienceDirect

Water Biology and Security

journal homepage: www.keaipublishing.com/en/journals/water-biology-and-security

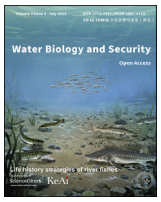

Research Article

Sex-biased miR-456 targeting spire1/sox11 provides insights into the ceRNA-network of sexual regulation in fish

Na Zhao [a,b,1], Xiaoxu He [c,1], Qianwen Min [b], Deborah Mary Power [d], Zhongdian Dong [a,**], Changgeng Yang [e,***], Bo Zhang [a,b,*]

[a] College of Fishery, Guangdong Ocean University, Zhanjiang, 524088, China
[b] Southern Marine Science and Engineering Guangdong Laboratory (Zhanjiang), Zhanjiang, 524000, China
[c] Tianjin Fisheries Research Institute, Tianjin, China
[d] Comparative Endocrinology and Integrative Biology, Centre of Marine Sciences, Universidade Do Algarve, Campus de Gambelas, Algarve, Faro, 8005-139, Portugal
[e] Life Science & Technology School, Lingnan Normal University, Zhanjiang, 524048, China

ARTICLE INFO

Keywords:
miR-456
spire1
sox11
ceRNAs
sex
Seriola dumerili

ABSTRACT

Competing endogenous RNAs (ceRNAs) are a novel epigenetic regulatory mechanism implicated in sex determination and differentiation in teleosts, which exhibit a diversity of sex-determining mechanisms. In this study, based on whole transcriptome sequencing data, a ceRNA regulatory network composed of sex-inclined miRNAs (miR-456), lncRNAs (*ASTR*), circRNAs (*circklhl29*), and target mRNAs (*spire1* and *sox11*) was uncovered in the gonadal tissues of *Seriola dumerili*, an oceanic species with lagged gonadal development. MiRNA-456 was identified as the core of the ceRNA regulatory network and suppressed the expression of *spire1* and *sox11*, interacting with the ncRNAs including *circklhl29* and *ASTR*. Co-localization of these sex-biased ncRNAs and mRNAs in the gonads suggests that this ceRNA network modulated the gonadal differentiation in both sexes of *S. dumerili*. *In vivo* injection in the gonads of *S. dumerili* suggested the miR-456 agonist could significantly inhibit expression of *sox11* and *spire1* in male testes, while significant regulatory effects of the miR-456 agonist and antagonist on *sox11* and *spire1* targets were not observed in female ovaries. The conserved binding sites for sequences of miR-456 and *spire1/sox11* targets in various fish species were aligned and dual luciferase reporter gene experiments clarified the universality of the mechanism by which miR-456 bound to inhibit *sox11/spire1* targets in large yellow croaker (*Larimichthys crocea*), half-smooth tongue sole (*Cynoglossus semilaevis*), and zebrafish (*Danio rerio*). These results further support the notion that ceRNA networks may be a universal regulatory system in teleosts despite their highly divergent sex regulation programs.

1. Introduction

The unique evolutionary and ecological circumstances of teleosts have resulted in a wide range of sex development patterns, which is made more complex since sex can be determined by genotypes or the environment. A number of genes affecting sex determination have been reported in different teleosts, such as *dmy* in *Oryzias latipes* (Chakraborty et al., 2016), *amhr2* in Tetraodontidae (Duan et al., 2021), *sdy* in *Oncorhynchus mykiss* (Brown et al., 2020), and *dmrt1, gsdf*, and *amh* in *Cynoglossus semilaevis* (Cui et al., 2017; Jiang et al., 2016; Li et al., 2015). Furthermore, epigenetic processes including DNA methylation, non-coding RNA (ncRNA) regulation, and the histone modification of chromatin structures can also play a role in sex differentiation in teleosts, which are sensitive to environmental changes (Deng et al., 2022; Zhang et al., 2019; Rui et al., 2024; Zhao et al., 2022; Jia et al., 2024; Li et al., 2024). ncRNAs are galleries of microRNAs (miRNAs), Piwi-interacting RNAs (piRNAs), long non-coding RNAs (lncRNAs), circular RNAs (circRNAs), ribosomal RNAs (rRNAs), transfer RNAs (tRNAs), nuclear small RNAs (snRNAs), and nucleolar small RNAs (snoRNAs), able to regulate gene expression at a post-transcriptional level. Several studies

* Corresponding author. College of Fishery, Guangdong Ocean University, Zhanjiang, 524088, China.
*** Corresponding author.
** Corresponding author.
E-mail addresses: zddong@gdou.edu.cn (Z. Dong), yangcg910@163.com (C. Yang), zb611273@163.com (B. Zhang).
[1] These authors contributed equally to this work.

https://doi.org/10.1016/j.watbs.2025.100370
Received 13 September 2024; Received in revised form 17 December 2024; Accepted 20 January 2025
Available online 23 January 2025

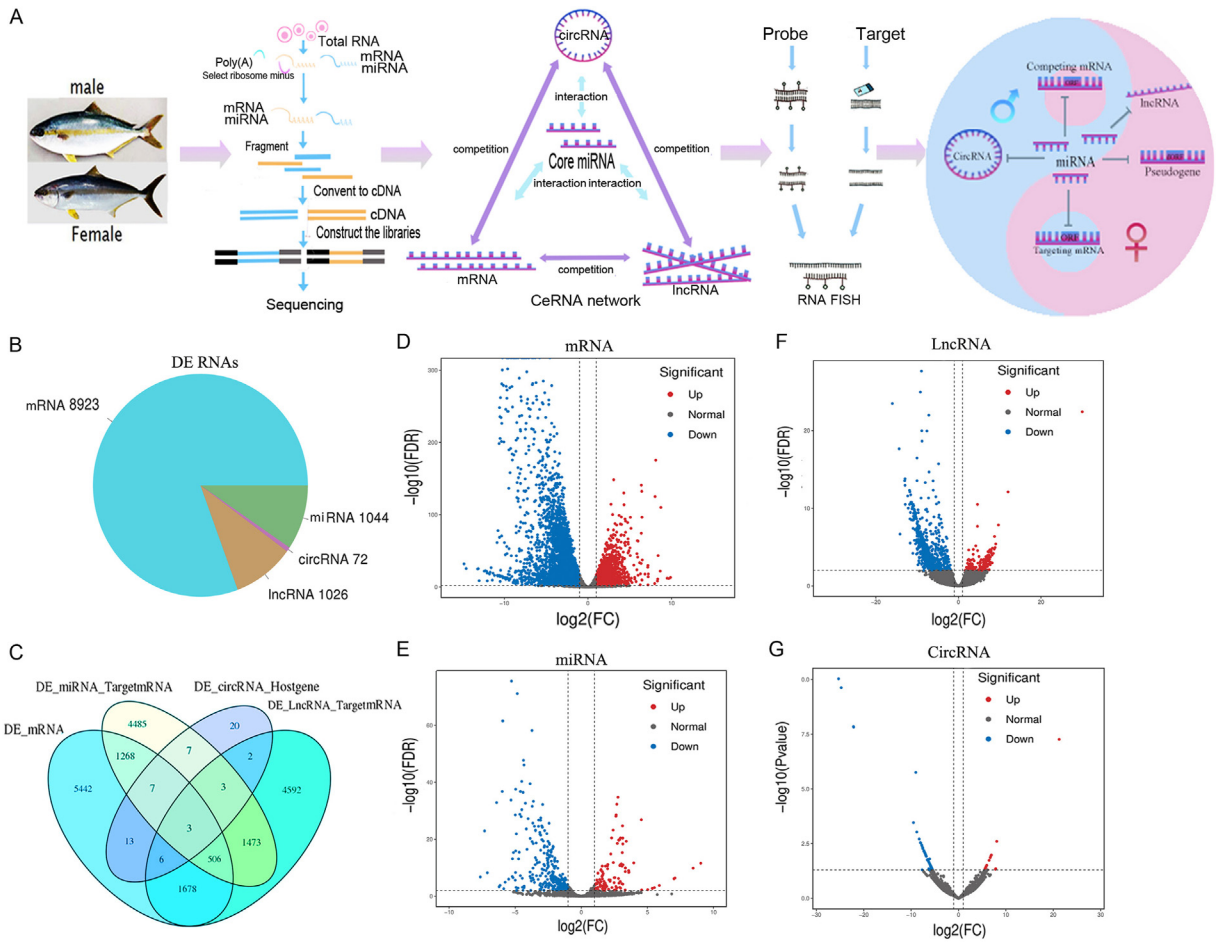

Fig. 1. Differentially expressed RNAs in the gonadal tissues of *S. dumerili*. (**A**) A general scheme of the experimental design. (**B**) The number of differential RNAs identified between the ovary and testis. (**C**) Venn diagram of differentially expressed mRNAs. (**D**) Volcano plot of differentially expressed mRNAs. (**E**) Volcano plot of differentially expressed miRNAs. (**F**) Volcano plot of differentially expressed lncRNAs. (**G**) Volcano plot of differentially expressed circRNAs. The *x*-axis represents the logarithm of the difference in the expression of the analyzed RNAs between the two sexes, and the *y*-axis represents the negative logarithm of the false discovery rate. The larger the *y*-axis value, the more significant the differential expression. The gray dots represent RNAs that were not differentially expressed, while the red dots and blue dots represent up-regulated and down-regulated RNAs, respectively.

have reported the differential expression of ncRNAs during sex differentiation in fish (Zhao et al., 2023; Huang et al., 2021); however, they mainly focused on the expression bias of ncRNAs or working mode of a single ncRNA type. MiR-133b was involved in the early oogenesis of tilapia (*Oreochromis nilotica*) and regulated the expression of *tagln2* (Ma et al., 2021). Dual luciferase reporter gene analysis of targets from *Opsariichthys bidens* confirmed the binding of miR-9-5p and *nanos1*, which was associated with the migration and differentiation of primitive germ cells (Tang et al., 2022). Sex reversal in *Epinephelus coioides* involved miR-26a-5p and *cyp19a1a* binding (Yu et al., 2020), while in *Takifugu rubripes*, miR-15b and novel miR_167 targeted *foxl2* and *dmrt1*, respectively (Yan et al., 2018). Thus, although ncRNAs play huge roles in fish sex differentiation, a comprehensive understanding of how different ncRNAs and their target genes work in an integrated network remains unexplored.

The coincident distribution and expression of ncRNAs and their target genes in differentiating gonadal tissues establishes the basis for an epigenetic action for competitive endogenous RNAs (ceRNAs) (B Zhang et al., 2020; Dong et al., 2021). CeRNAs are a class of RNAs that bind competitively to molecular binding sites in miRNAs and affect their regulatory action on the expression of target genes, such as lncRNAs and circRNAs (Karreth et al., 2015; Wang et al., 2016; Yu et al., 2015; Ning et al., 2024). For example, Li et al. (2021) constructed a core circRNA-miRNA-mRNA interaction network related to testicular function in sheep (*Ovis aries*) and identified circ_024949, circ_026259, IGF1, and miR-29b in the network, revealing their similar expression characteristics in the developing testis and their influence on the development and maturation of male germ cells. In *Monopterus albus*, circ*Snd 1* regulated *foxl2* by serving as a sponge of miR-135 b/c (He et al., 2022), and lncRNA *DMRT2-AS* promoted the expression of *dmrt2* at the transcriptional level during male gonadal differentiation (Feng et al., 2021), but no ceRNA network was constructed. In *C. semilaevis,* Tang et al. (2022a) demonstrated that a ceRNA network involving circdmrt 1 and lncRNA-*AMSDT* eliminated the endogenous inhibitory effect of cse-miR-196 on the target gene *gsdf* and triggered the male sex determination pathway (Tang et al., 2022a). Research on Nile tilapia (*Oreochromis nilotica*) and common carp (*Cyprinus carpio*) has also suggested the regulatory effects of lncRNAs and circRNAs on miRNAs and the expression of sex-related genes such as *hsd17β3* (Zhong et al., 2022; Hou et al., 2023). However, ceRNA network-related research is still limited, especially in fish.

Greater amberjack (*Seriola dumerili*) is an emerging farmed oceanic species that grows fast, and female greater amberjacks, which are the heterogametic sex (ZZ/ZW), mature at about 3–4 years of age (Kawase et al., 2018). Compared to wild fish, the gonad development in cultured greater amberjack is sluggish, the gametes are of poor quality, and the gonads are readily reabsorbed (Papadaki et al., 2021; Sarropoulou et al., 2017; Kawase et al., 2018; Deng et al., 2023; Zupa et al., 2017; Fakriadis et al., 2020; Perez et al., 2020; Corriero et al., 2021). The strong influence

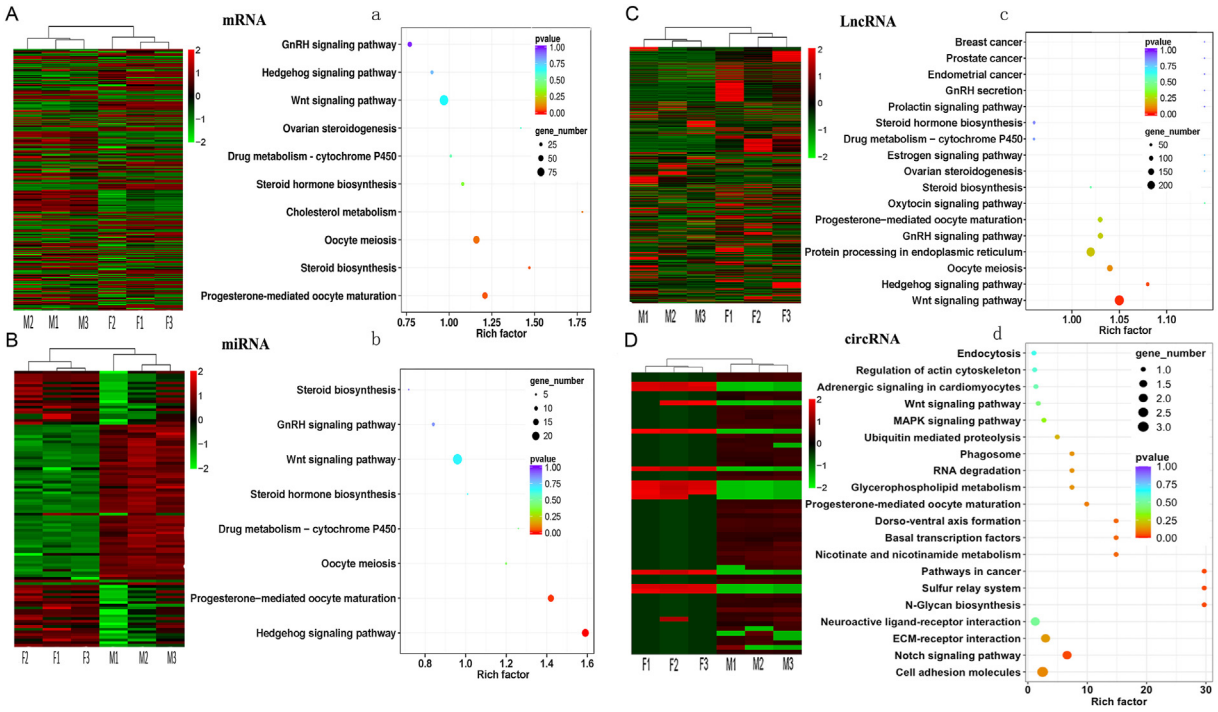

Fig. 2. Heatmap and the predicted function of differentially expressed (DE) RNAs between the ovary and testis from *S. dumerili*. (**A**) Sex-biased mRNAs, (**B**) miRNAs, (**C**) lncRNAs, and (**D**) circRNAs (the circRNAs in the red boxes are sex-related). The threshold for the identification of DE RNAs was set at $P < 0.05$ and $|\log_2$ fold change$| > 2$. Individuals are indicated as F1–3 (females) and M1–3 (males) along the *x*-axis, and the up- and down-regulation of DE RNAs is indicated by differing intensities of red and green as indicated in the side-scale of each heatmap. The KEGG pathways that were enriched in the sex-biased DE RNAs are given for (**a**) mRNAs, (**b**) miRNAs, (**c**) lncRNAs, and (**d**) circRNAs. In the KEGG pathway plots the *x*-axis represents the enrichment score, while the *y*-axis represents the name of the KEGG pathway. The bubble color represents the *P*-value and the size represents the number of genes involved in the pathway.

of the environment on female gonad development and the poor quality of the gametes limits the sustainability of this species in aquaculture. To date, there is not much research on the sex differentiation of oceanic fish including *S. dumerili*, especially on ncRNAs-related mechanisms (Zhao et al., 2023), let alone ceRNA networks. To contribute to the resolution of this problem, the epigenetic regulation mechanism of gonad development in *S. dumerili* was characterized. CeRNA networks in differentiating gonadal tissues of males and females were constructed, and the role of sex-biased ncRNAs mediating ceRNA crosstalk was identified to provide insight into the epigenetic mechanisms of sex differentiation in this fish.

2. Materials and methods

2.1. Sampling

The cultured one-year-old *S. dumerili* used in our experiment were purchased from the Fuminyang fish farm (Zhangzhou, Fujian, China). Fish were kept in captivity in open-air fish rafts, and the water temperature was 28 °C. Six fish were sacrificed by administering an overdose of eugenol (100 mg/L) in water. There were no significant differences in body length (L) and weight (Wt) between these three males and three females (male L: 41.3 ± 0.9 cm, Wt: 1166.67 ± 94.28 g; female L: 41.9 ± 1.3 cm, Wt: 1216.64 ± 164.99 g; independent sample *t*-test, $P > 0.05$). Gonad samples from these three females (GSI = 0.07% ± 0.03%) and three males (GSI = 0.13% ± 0.04%) were collected, and each gonad was divided into two parts. One half was flash-frozen in liquid nitrogen and stored at −80 °C until RNA extraction and sequencing, and the other part was fixed in RNase-free 4% paraformaldehyde fixative (PFA) for at least 24 h at 4 °C with occasional agitation and was used for histology.

2.2. Construction and sequencing of RNA libraries

RNA was extracted from the frozen male and female gonads using a Trizol total RNA extraction kit (Guangzhou Dongsheng Biotech Co., Ltd (GDSBio), Guangzhou, China). The extracted total RNA was treated with DNase. The quantity and quality of the DNase-treated total RNA were determined using an Agilent 2100 biological analyzer and an RNA 6000 Nano LabChip Kit (Agilent, Santa Clara, USA). An epicenter Ribo ZeroTM reagent kit was used to remove rRNA and a fragmentation buffer was added to randomly interrupt rRNA-dissected RNA. For full transcriptome sequencing, six libraries for small RNA determination (miRNA) and six ribosome-free strand-specific libraries (3 for male and 3 for female gonads in both cases) for mRNA, lncRNA, and circRNA were constructed separately. Using rRNA-depleted RNA as a template, cDNA libraries were obtained through PCR amplification (Li et al., 2021). Sequencing of the small RNA library and the strand-specific library were carried out using an Illumina HISEQ 2500 platform (Biomark Biotechnology Co., Ltd., Beijing). Paired-end reads of 150 bp and single-end reads of 50 bp were obtained in FASTQ format.

2.3. Bioinformatics analysis of sequences

2.3.1. Ribosome-free strand-specific libraries

The raw sequence reads for the ribosome-free strand-specific libraries were filtered to remove adaptors, low-quality sequences, and contaminating ribosomal RNA sequences. For lncRNA/mRNA filtering and annotation analysis, HISAT2 software (v2.1.0) (Kim et al., 2019) was used. StringTie (v1.3.5) (Pertea et al., 2016) software was used for assembly, while CIRI (Gao et al., 2015) and find_circ (Memczak et al., 2013) software were used to predict and identify circRNAs.

2.3.2. miRNA libraries

Sequences shorter than 18 or longer than 30 nucleotides were removed from the miRNA library using Bowtie2 software (v2.5.1) (Langmead et al., 2009). Sequence alignments were performed on clean reads using the Silva ribosomal RNA database (http://www.arb-

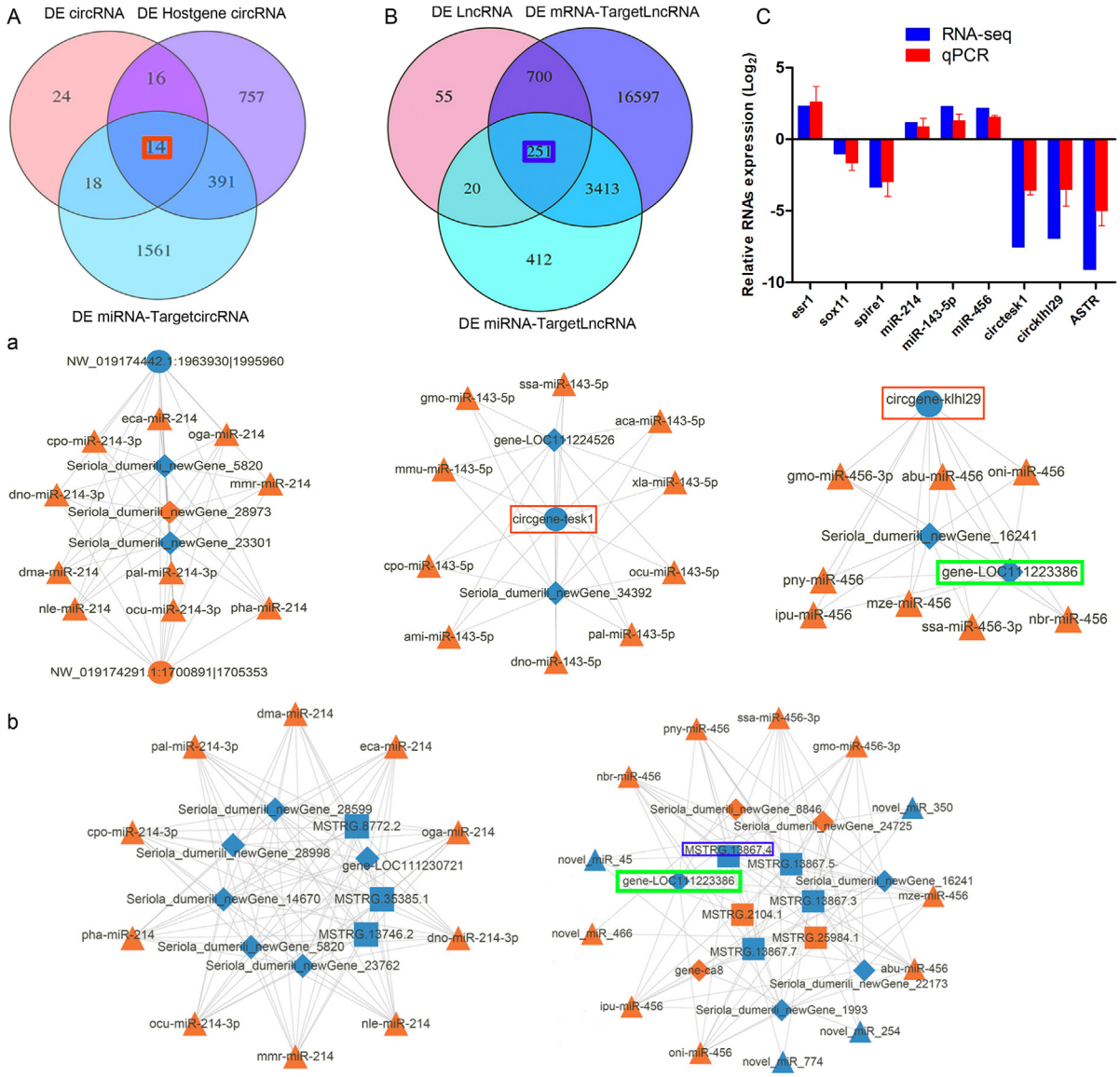

Fig. 3. CeRNA interaction networks among differential ncRNAs and targets, and qRT-PCR validation of core sex-biased RNAs. (**A**) Venn analysis of differentially expressed (DE) circRNAs, DE Hostgene circRNAs, and DE miRs targetcircRNAs which identified 14 common circRNAs. (**a**) The three ceRNA networks constructed using the sex-biased circRNA-miRNA-mRNA identified by Cytoscape. The gene symbol of LOC111224526, LOC111223386 in (a), and LOC111230721 in (b) was *sema3aa*, *spire1*, and *tmem106c*, respectively. (**B**) The Venn analysis of DE lncRNAs, DE mRNA targetlncRNA, and DE miRNA target lncRNA identified 251 lncRNAs at the intersection of the three groups. (**b**) Two ceRNA networks identified when the sex-biased lncRNA-miRNA-mRNA were analyzed by Cytoscape. (**C**) Real-time quantitative PCR (qRT-PCR) analysis of differentially expressed sex-related RNAs. The relative expression between the ovary and testis (log transformed) is shown. The blue bars show the value of $\log_2$Foldchange from RNA-seq and the red bars show the relative expression of RNAs by qRT-PCR. The data represent the mean ± standard deviation (n = 3). Note: in (a) and (b), the triangles represent miRNA, the circles circRNA, the squares lncRNA, and the diamonds mRNA. The shapes shaded in orange represent up-regulation and those shaded in blue represent down-regulation in the ovary compared to the testis.

silva.de/), GtRNAdb database (http://lowelab.ucsc.edu/GtRNAdb/), Rfam database (http://rfam.xfam.org/), and Repbase database (http://www.girinst.org/repbase/). rRNA, tRNA, snRNA, snoRNA, and other ncRNAs, as well as repeat sequences, were removed by filtering to obtain unannotated reads containing miRNA. Sequences were "polished" to obtain consistent sequences by aligning them with the reference genome of *S. dumerili* (GCF_002260705.1) and redundant sequences were removed. The reads aligned with the reference genome were compared with the mature sequences of known miRNAs and their upstream 2 nt and downstream 5 nt ranges using miRBase (v22) (Griffiths-Jones et al., 2006), and sequencing reads corresponding to known miRNAs were identified. For unidentified sequences, Bayesian models were used to predict novel miRNAs based on precursor sequences and RNA fold information obtained using miRDeep2.0.5 software (Friedlander et al., 2012).

2.3.3. Differential expression analysis

The FoldChange was the ratio of the level of expression of miRNA and mRNA, lncRNAs, and circRNAs between the male and female samples, and the FDR (False discovery rate) was obtained by using the Benjamini Hochberg procedure to correct the *P*-values. The target genes of differentially expressed miRNAs, lncRNAs, and circRNAs were predicted using miRanda v3.3a (Enright et al., 2003) with the parameters $S \geq 150$, $\Delta G \leq -30$ kcal/mol, and Demand strict 5' seed pairing. R software was used to plot Venn diagrams, heatmaps, and volcano plots. GO and KEGG pathway enrichment analysis of differentially expressed genes (DEGs) and predicted target genes of miRNAs and lncRNAs were performed (Deng et al., 2022), and a Benjamini & Hochberg procedure was performed on the

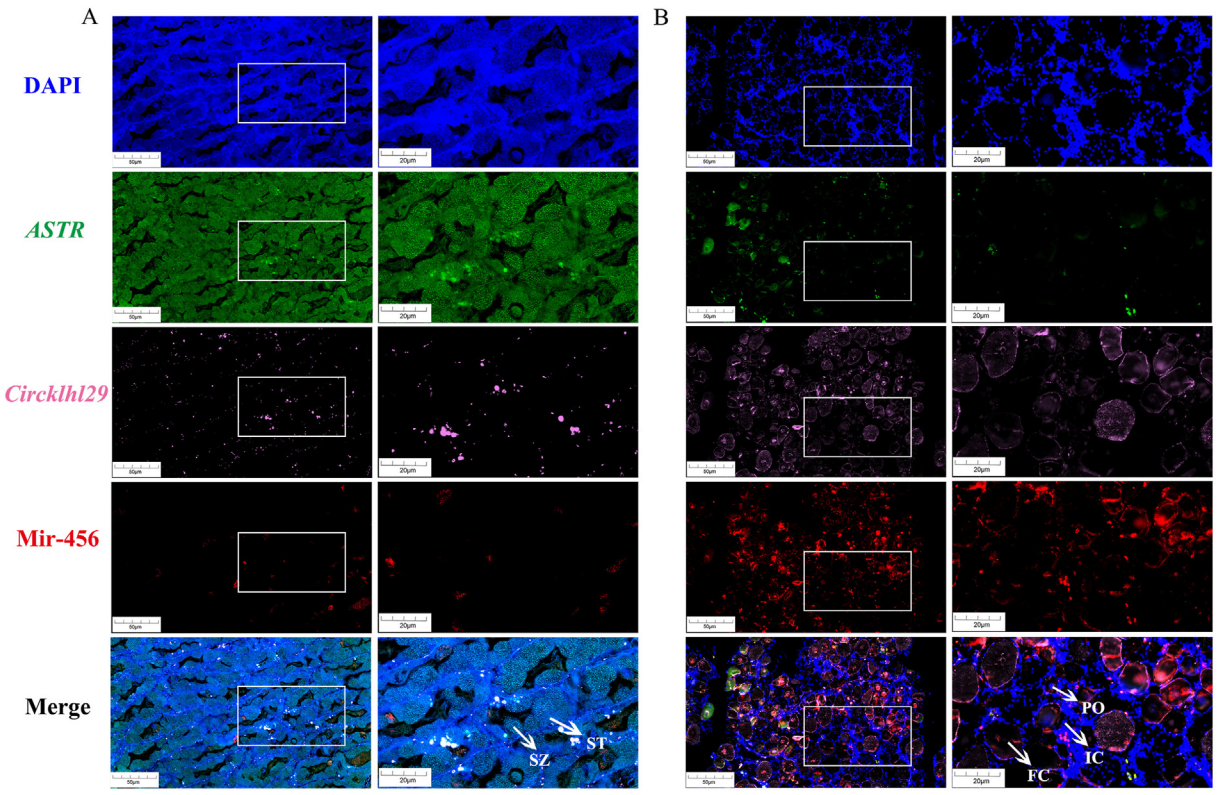

Fig. 4. RNA fluorescence in situ hybridization (FISH) of the miR-456-*circklhl29-ASTR* with three color markers. (**A**) RNA FISH for the miR-456-*circklhl29-ASTR* in paraffin sections of *S. dumerili* testis. The panel shows the localization of DAPI and each of the target RNAs individually followed by a merged image. (**B**) RNA FISH for the miR-456-*circklhl29-ASTR* in paraffin sections of *S. dumerili* ovary. The panel shows the localization of DAPI and each of the target RNAs individually followed by a merged image. DAPI was used to stain the nucleus, and the RNA probes localized *lncASTR* (FAM, green), miR-456 (CY3, red light), and *circklhl29* (CY5, pink). The fluorescence intensity differed according to the expression level of the target RNAs. Abbreviations: (ST) spermatocyte, (SZ) spermatozoa, (FC) follicle cavity, (IC) Interstitial cells, (PO) primary oocyte. The scale of each graph on the left was 50 μm, while the scale of each graph on the right was 20 μm.

P-values to correct the false discovery rate (FDR). RNAhybrid v2.1.1 (Rehmsmeier et al., 2004), miranda (Betel et al., 2008), and TargetScan (Lewis et al., 2003) were used to predict the targeting relationships between differentially expressed circRNAs, mRNAs, and miRNAs. A Pearson correlation coefficient (R) was used to calculate the strength of the correlation between differentially expressed miRNAs and their putative targets. The cut-off value set for the selection of candidate circRNA-miRNA, miRNA-mRNA, lncRNA-miRNA, and lncRNA-mRNA pairs was $P < 0.05$ and $R > |0.8|$. The targeting relationships, co-occurrence, and expression level of ceRNAs were all taken into account during the ceRNA network construction process. When the number of identical miRNAs between ceRNAs was greater than 3, and the *P*-value of the hypergeometric test with the corrected FDR value was less than 0.01, a ceRNA co-expression network with pairwise co-expression between ceRNAs was obtained. The circRNA-miRNA-mRNA and lncRNA-miRNA-mRNA networks were constructed using Cytoscape v3.9.1 (Shannon et al., 2003).

2.4. qRT-PCR verification of differentially expressed RNA

Total RNA extracted from the male and female gonads was also used for quantitative PCR (qRT-PCR) of candidate binding partners, which were chosen from hub genes of the networks and the sex-related genes including *esr1*, *spire1*, *sox11*, miR-214, miR-143-5p, miR-456, *circtesk1, circklhl29*, and *ASTR*. Total RNA extracted from *S. dumerili* gonads ($n = 3$ for male and $n = 3$ for female) was reverse transcribed into template cDNA using a HiFiScript cDNA first-strand synthesis kit (CWBIO, Jiangsu, China). The reference genes selected for qRT-PCR analysis all had a constant expression across the samples and they were specific for each type of RNA studied, including mRNA (*actb2*), miRNA (*tni-miR-100*), circRNA (*newGene17096_11*), and lncRNA (*MSTRG.17244.2*). The qRT-PCR was carried out using a StepOnePlus real-time quantitative PCR instrument (Applied Biosystems) and a SYBR FAST qPCR Kit Master Mix (2×) (KAPA Biosystems, KK4601) with specific primers designed for each target RNA (supplementary file 1). The thermocycle for all reactions was as follows: 95 °C for 3 min, then 40 cycles of 95 °C for 10 s and 60 °C for 30 s, and a final melt curve to check single reaction products. All qRT-PCR reactions were performed with three technical replicates and the expression level was calculated using the $2^{-\Delta\Delta Ct}$ formula (Livak and Schmittgen, 2001).

2.5. Histological analysis and RNA fluorescent in situ hybridization

For histological analysis, the gonad tissue was fixed in 4% PFA, stored in 70% ethanol dehydrated through gradient alcohol (70%, 80%, 90%, 95%, and 100%), saturated with xylene, and then infiltrated with low melting point paraffin wax (Sakura, Japan. The wax-embedded male and female gonads were sectioned (5 μm) using a Leica manual microtome, mounted on slides, and dried in an oven at 40 °C. The general histology of the sectioned gonads was determined using hematoxylin and eosin staining and they were mounted on a neutral gum-covered glass slide. A Nikon ECLIPSE Ni (Nikon, Japan optical microscope was used to observe and photograph the slides.

Fluorescent in situ hybridization (FISH) was carried out using tissue sections of *S. dumerili* testes and ovaries and specific antisense probes for *spire1, sox11, circklhl29, ASTR*, and miR-456 fragments (supplementary file 2). The following fluorochromes (Servicebio, Wuhan, China) were selected for the different probes: *spire1* and *lncASTR* were linked to FAM (FAM maleimide, 6-isomer), which emitted green light (excitation wavelength of 465–495 nm/emission wavelength of 515–555 nm); MiR-

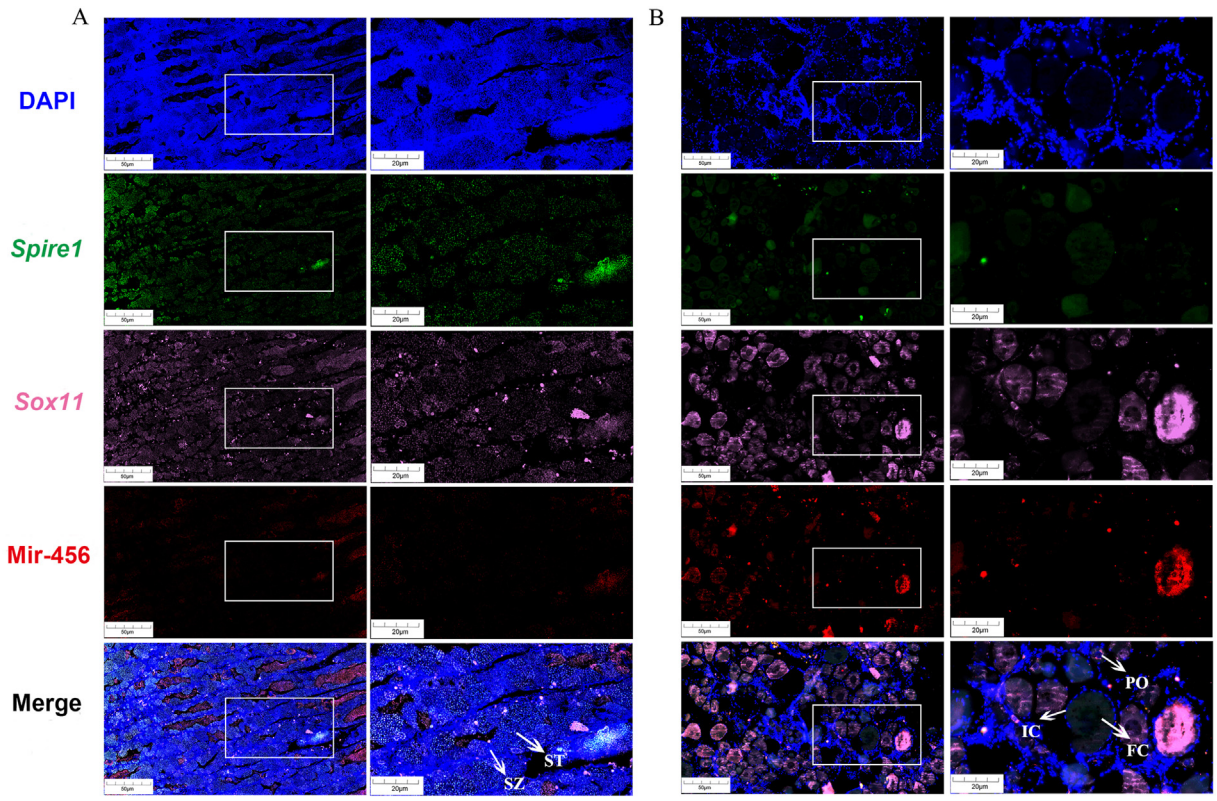

Fig. 5. RNA fluorescence in situ hybridization (FISH) of miR-456-*sox11-spire1* (**A**) RNA FISH for the miR-456-*sox11-spire1* in paraffin sections of *S. dumerili* testis. The panel shows the localization of DAPI (used to stain the nucleus) and each of the target RNAs individually and then as a merged image. (**B**) RNA FISH for the miR-456-*sox11-spire1* in paraffin sections of *S. dumerili* ovary. The panel shows the localization of DAPI and each of the target RNAs individually and then as a merged image. The RNA probes localized *lncASTR* (FAM, green), miR-456 (CY3, red light), and *circklhl29* (CY5, pink). The fluorescence intensity differed according to the expression level of the target RNAs. Abbreviations: (ST) spermatocyte, (SZ) spermatozoa, (FC) follicle cavity, (IC) Interstitial cells, (PO) primary oocyte. The scale of each graph on the left was 50 μm, while the scale of each graph on the right was 20 μm.

456 was linked to CY3 (Cyanine3) emitting red light (excitation 510–560 nm/emission 590 nm); and *sox11* and *circklhl29* were linked to CY5 (Cyanine5) with pink light (excitation 648 nm/emission 662 nm). The main steps for FISH included pre-hybridization (in 2 × SSC, 50% formamide deionized, 1% BSA, 1 M Tris-HCl, 0.5 M EDTA) for 1 h at 37 °C, and hybridization with a pre-hybridization buffer containing a 500 nM probe overnight at 42 °C. Slides were then washed in SSC buffer (SSC: 3 M NaCl, 0.3 M sodium citrate (pH = 7)) at different concentrations to remove the non-specifically annealed probe (1: wash sections with 2 × SSC for 5 min at 37 °C; 2: wash sections in 1 × SSC two times for 5 min each at 37 °C; and 3: wash in 0.5 × SSC for 10 min at room temperature). After washing, the slides were stained with DAPI (4′,6-diamidino-2-phenylindole) (Servicebio, Wuhan, China), incubated with the solution in the dark for 8 min, and then sealed with a non-quenching sealing agent. Sections were observed and photographed under a Nikon ECLIPSE CI (Nikon, Japan upright fluorescence microscope.

2.6. Vector construction and dual luciferase reporter assay

Based on the 3′UTR sequence of *spire1, sox11, circklhl29,* and *ASTR* of *S. dumerili*, the wild type (WT) and the mutant type (MT) sequences, as well as *spire1* and *sox11* of large yellow croaker (*Larimichthys crocea*), half-smooth tongue sole (*C. semilaevis*), and zebrafish (*Danio rerio*) were synthesized (Entrust genecreate, Wuhan, China). The purified PCR products of target fragments were cloned into pmirGLO vectors (Solarbio). For transfection of 293T cells with the vector constructs, the cells in DMEM (ThermoFisher, USA) medium containing 10% FBS were plated at a density of 1×10^5 cells/well and incubated for 24 h at 37 °C in a Forma 3111 (ThermoFisher, USA). For transfection, 2 μg plasmid (recombinant pGL3-basic containing PCR products) and 50 nmol/L miRNA in 50 μL serum-free DMEM medium were incubated at room temperature for 5 min, and then Lipofectamine 2000 (2 μL), the transfection reagent (Invitrogen), and serum-free DMEM (500 μL) were added. The reporter assay was performed for 24 h after transfection using a dual Luciferase Reporter Gene Assay Kit (Beyotime, Shanghai, China) for double fluorescence reporter gene detection. Renilla luciferase was used as the internal reference, and the activation of the reporter gene was determined by the ratio of the luminescence of firefly luciferase Fto the luminescence of Renilla luciferase (as relative light units (RLU)

2.7. In vivo injection AGO/ANTAGO-miR-456 into the gonads of S dumerili

The one-year-old *S. dumerili* were divided into four groups: NC agomir, miR-456 agomir, NC antagomir, and miR-456 antagomir, with three males and three females in each group. Food intake was suspended for one day before surgery. We transferred the fish into a bucket containing 40 mg/L eugenol as an anesthetic for 5 min. We then used scissors (disinfected with alcohol) to cut a small 1–2 cm opening anterior from the urogenital opening to locate the gonads. We inserted a needle into the gonads and rapidly injected 1 nmol of NC agomir, miR-456 agomir, NC anatgomir, or miR-143 antagomir solution into each fish. We then disinfected the abdominal incision with alcohol swabs, aligned the incision with tweezers, added two drops of 3M Vetbond biological tissue adhesive (Minnesota Mining and Manufacturing Company, MN, USA), and continued holding the incision with tweezers for 90 s until the adhesive dried. Then we transferred the fish to a circulating water system, and after 5 h sacrificed the fish to collect their gonads.

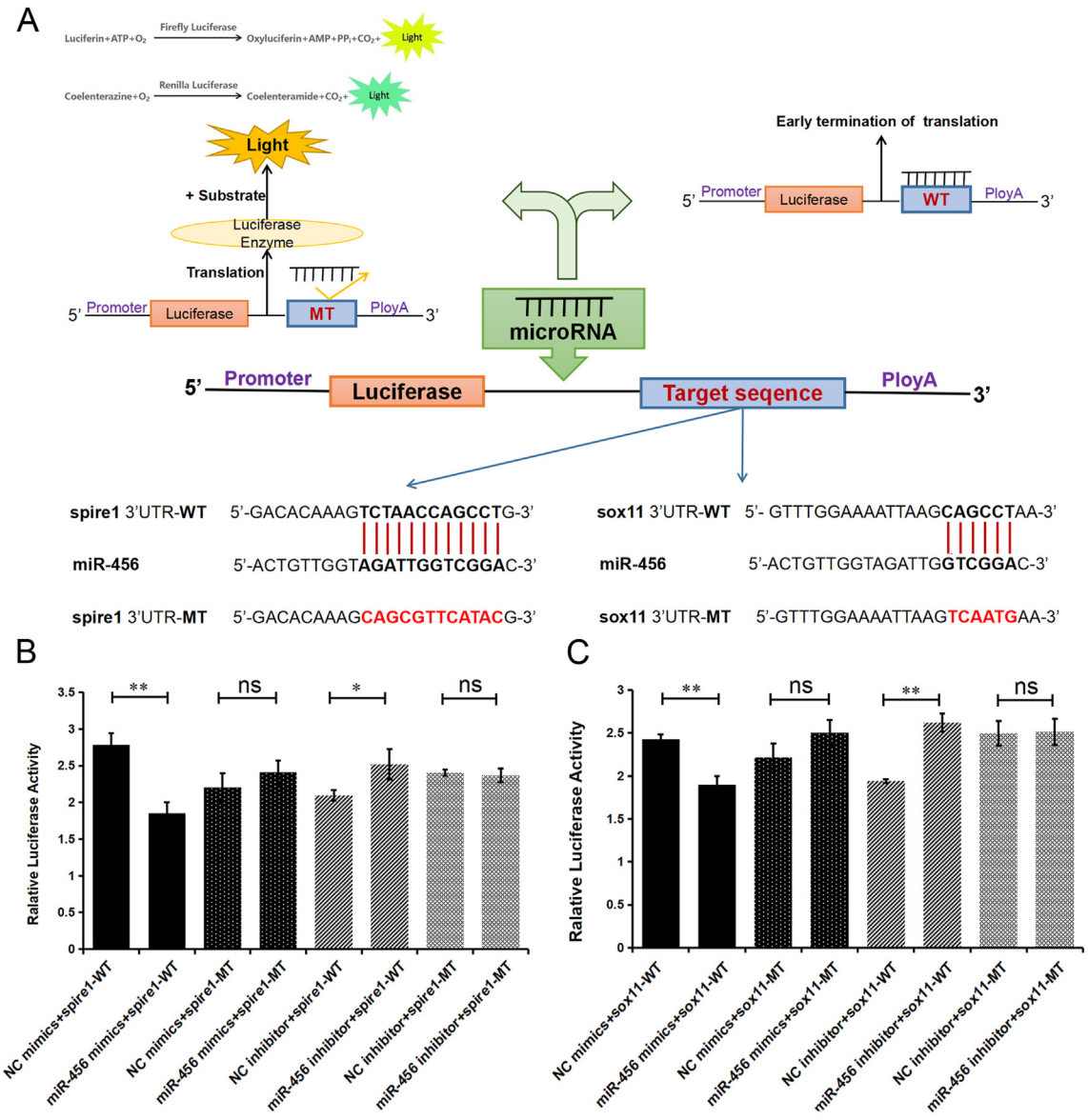

Fig. 6. Detection of dual luciferase activity of miR-456 with *spire1* and *sox11* in 293 T cells. (**A**) A schematic diagram of the dual-luciferase reporter gene detection. The red lines indicate the binding sites of miR-456 to *spire1* 3′UTR-WT and *sox11* 3′UTR-WT and the red bases represent the mutated binding sites in the modified gene. (**B**) The results of the dual-luciferase activity detection of miR-456 and *spire1* in transfected 293 T cells. (**C**) The results of dual-luciferase activity detection of miR-456 and *sox11* in transfected 293 T cells. The plasmid constructs used for transfection in the 293 T cells are on the *x*-axis and the relative luciferase activity is on the *y*-axis. Data are represented as the mean ± standard deviation ($n = 3$ assays). The significance level is indicated, $^{*}P < 0.05$, $^{**}P < 0.01$, and ns represents $P > 0.05$.

2.8. Statistical analysis

Data from qRT-PCR and dual luciferase reporter experiments are presented as the mean and standard deviation of triplicates for each sample. Student's *t*-tests for independent samples were used to evaluate if there were significant differences between groups using SPSS 25.0 software. Significance was assessed at $P < 0.05$(*) and $P < 0.01$(**).

2.9. Data availability

The raw data can be found in online repositories. The data were uploaded to the NCBI under accession number PRJNA951502 (https://www.ncbi.nlm.nih.gov/bioproject/PRJNA951502).

3. Results

3.1. Expression profiles of mRNA and ncRNA in both female and male gonadal tissues

A total of 70.53 Gb clean data were obtained for long-chain non-coding RNA analysis. Clean data for each sample reached 11.44 Gb, and the Q30 base percentage was greater than 94.58%. The clean reads aligned to the reference genome in female samples were in the range of 64,380,291 (82.23%) to 68,718,523(89.72%) for each individual fish, while in the male group they ranged from 73,748,036 (95.45%) to 76,467,134 (94.90%) for individual fish. A total of 34,872 mRNAs, 3565 miRNAs, 4703 circRNAs, and 24,190 lncRNAs were identified by high-

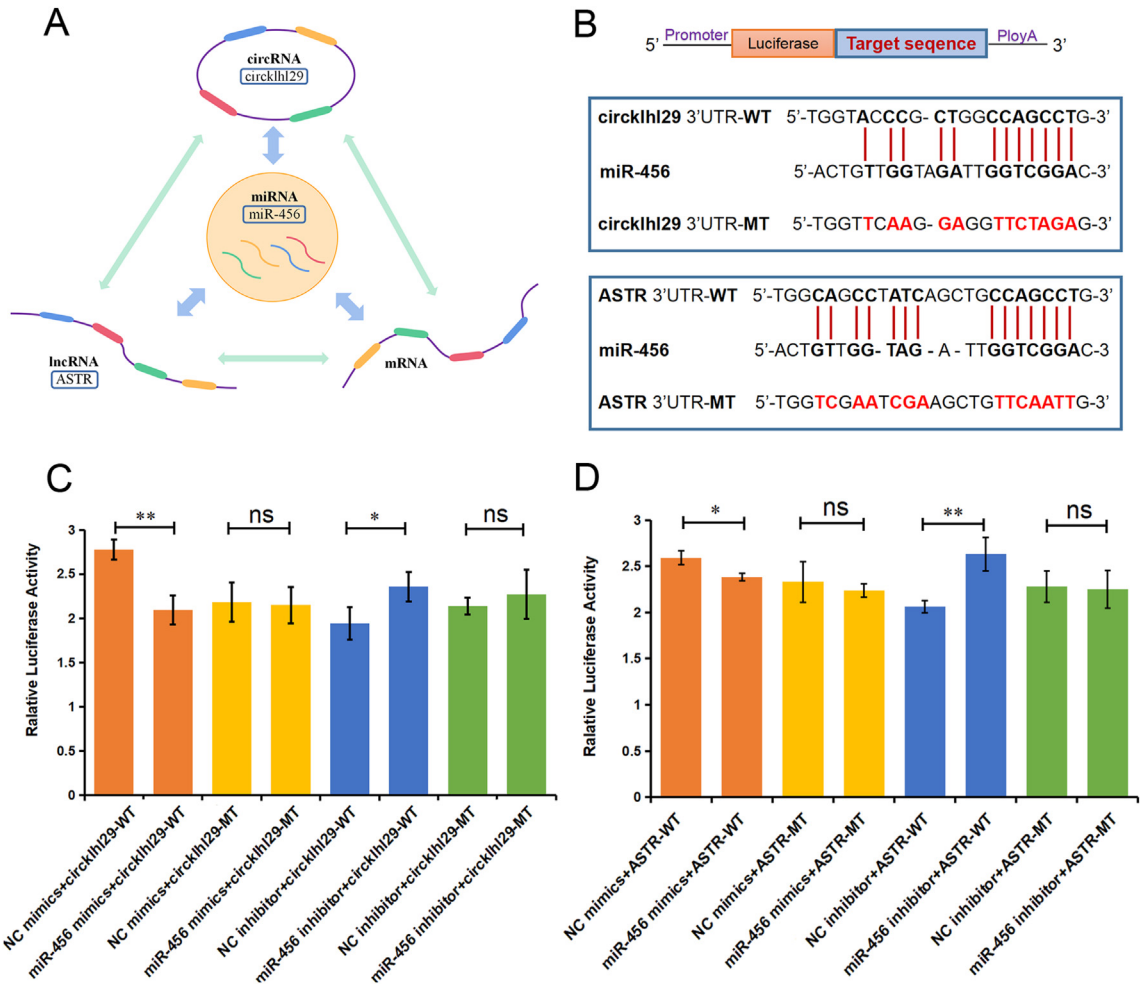

Fig. 7. Detection of dual luciferase activity of miR-456 with *circklhl29* and *ASTR* in 293T cells. (**A**) The principle schematic diagram of the target gene and ncRNA interaction. (**B**) Diagram of double luciferase reporter gene detection binding site (red line points to the binding sites of miR-456 with *circklhl29* 3′UTR-WT or *ASTR* 3′UTR-WT, and red bases represent the mutated binding sites in the modified gene). (**C**) Double luciferase activity detection results of miR-456 and *circklhl29* in transfected 293 T cells. (**D**) Double luciferase activity detection results of miR-456 and *ASTR* in transfected 293 T cells. The plasmid constructs used for transfection in the 293 T cells are on the x-axis and the relative luciferase activity is on the y-axis. Data are represented as the mean ± standard deviation ($n = 3$ assays). The significance level is indicated, $^{*}P < 0.05$, $^{**}P < 0.01$, and ns represents $P > 0.05$.

throughput sequencing.

The genome-wide differential RNA analysis between the ovary and testis identified 8923 differentially expressed mRNAs (DE mRNAs), 1044 differentially expressed miRNAs (DE miRs), 72 differentially expressed circRNAs (DE circs), and 1026 differentially expressed lncRNAs (DE lncs) (Fig. 1B). Venn analysis was carried out with the DE mRNAs, the targets of DE miRs and DE lncs, and the source genes of the DE circs (Fig. 1C). Comparison of DE mRNAs between the ovary and testis revealed 3678 and 5245 genes significantly upregulated and downregulated, respectively, in females (Fig. 1D). Similarly, the expression of 506 DE miRs were significantly higher and 538 were significantly lower in the ovary compared to the testis (Fig. 1E). A total of 1026 DE lncs were identified, of which 182 had a significantly higher expression in the ovary (Fig. 1F). Among the DE circs, 15 were higher in the ovary while 57 were higher in the testis (Fig. 1G).

3.2. Enrichment analysis of the KEGG pathway of sex-biased RNAs

The expression levels of sex-related differentially expressed mRNAs, miRNAs, lncRNAs, and circRNAs are shown in Fig. 2A–D, respectively. A total of 260 DE mRNAs were enriched in reproductive endocrine-related pathways, including 122 ovary-biased and 138 testis-biased ones. The top enriched pathways included progesterone-mediated oocyte maturation, steroid biosynthesis, oocyte meiosis, cholesterol metabolism, drug metabolism-cytochrome P450, ovarian steroidogenesis, Wnt signaling, Hedgehog signaling, and GnRH signaling (Fig. 2a). The target genes of 103 sex-related DE miRNAs were enriched into eight KEGG pathways, including the Hedgehog signaling pathway, progesterone-mediated oocyte maturation, and oocyte meiosis (Fig. 2b). There were 1026 sex-biased lncRNAs including 182 ovary-biased and 844 testis-biased ones, and the targets of these lncRNAs were enriched into pathways including the Wnt signaling pathway, Hedgehog signaling pathway, and oocyte meiosis (Fig. 2c). Host genes of the 72 annotated DE circRNAs were assigned to pathways such as cell adhesion molecules, Notch signaling, progesterone-mediated oocyte maturation, Wnt signaling, and MAPK signaling (Fig. 2d).

3.3. Construction of ceRNA regulatory networks and qRT-PCR validation of core sex-biased RNAs

Venn analysis of DE circRNAs, DE_hostgene_circRNAs (circRNAs whose Hostgenes were differential expressed mRNAs), and DE miR-targeting circRNAs (circRNAs targeted by differential miRNAs) had a total of 14 common circRNAs (Fig. 3A). The circRNA-miRNA-mRNA networks were constructed and ovary-biased miR-214, miR-143-5p, and miR-456 were identified (Fig. 3a). The 14 intersecting circRNAs

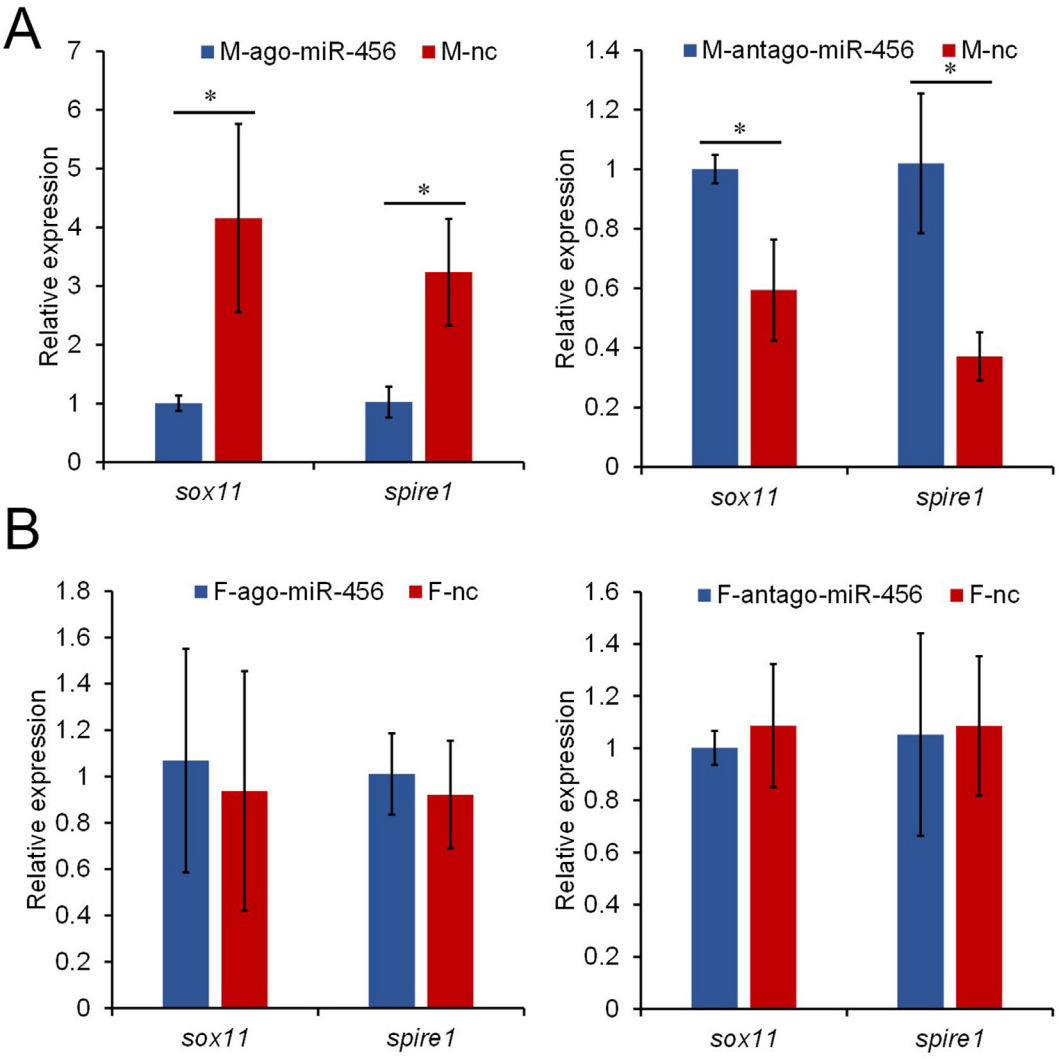

Fig. 8. qRT-PCR testing of the expression level of targets *sox11* and *spire1* of both testis and ovary in *S. dumerili* under agonist/antagonist miR-456 injection *in vivo*. (**A**) The expression levels of target genes in male testes injected with an agonist (left-sided panel) and an antagonist (right-sided panel). M-ago-miR-456 represents the agonist-miR-456; M-antago-miR-456 represents the antagonist-miR-456; and M-nc represents the control group NC-miR-456. (**B**) The expression levels of target genes in female ovaries injected with an agonist (left-sided panel) and an antagonist (right-sided panel). F-ago-miR-456 represents the agonist-miR-456; F-antago-miR-456 represents the antagonist-miR-456; and M-nc represents the control group NC-miR-456. Names of target genes are on the *x*-axis and the relative expression level is the *y*-axis. Data are represented as the mean ± standard deviation ($n = 3$ assays). The significance level is indicated, $^{*}P < 0.05$, $^{**}P < 0.01$.

contained only two known circRNAs, circle-klhl29 and circle-tesk1. The intersection of DE lncRNAs, DE mRNA-targeting lncRNAs (lncRNAs whose targets were differential mRNAs), and DE miR-targeting lncRNAs (lncRNAs who were targeted by differential miRNAs) identified 251 shared lncRNAs (Fig. 3B). LncRNA-miRNA-mRNA networks were constructed with ovary-biased miR-214 and miR-456 as the center (Fig. 3b). MiR-456, circgene-*klhl29*, and *ASTR* (MSTRG.13867.4) were all predicted to target *spire1* (gene-LOC111223386 in Fig. 3a) in the two networks identified, indicating a complex regulatory interaction among the four RNAs. The expression levels of the identified miRNAs (miR-214, miR-143-5p, and miR-456) and their sex-related target genes (*esr1, sox11,* and *spire1*), as well as circRNAs (circle-*tesk1* and circle-*klhl29*) and the lncRNA (*ASTR*), were analyzed by qRT-PCR. The results were consistent with the differential RNA expression profiles obtained by sequencing (Fig. 3C). Except *esr1*, expression levels of the other RNAs were negatively correlated with the miRNAs, with a lower expression level in females.

3.4. Co-localization of miR-456-circklhl29-lncASTR and miR-456-sox11-spire1 in the testis and ovary

RNA fluorescence in situ hybridization (RNA FISH) was used to assess the localization of miR-456-*circklhl29-lncASTR* in the testis and miR-456-*sox11-spire1* in the ovary of *S. dumerili*. We found that miR-456-*circklhl29-lncASTR* was primarily co-localized and co-expressed in the spermatocytes and spermatozoa in the testis, while miR-456-*sox11-spire1* was co-localized in the follicle cavity and interstitial cells of the ovary. Furthermore, the fluorescent signal of *lncASTR* was significantly more abundant in the testis than in the ovary (Fig. 4A), while miR-456 fluorescence was more abundant in the ovary (Fig. 4B). *Circklhl29* was mainly distributed in the spermatocyte (Fig. 4A), although it was also detected with low abundance in the follicular cavity of the ovary (Fig. 4B). In the merged image of miR456-*sox11-spire1*, the fluorescence signal of *spire1* was more abundant in the testis (Fig. 5A), while the fluorescence signal of miR-456 was more abundant in the ovary (Fig. 5B). *sox11* was mainly

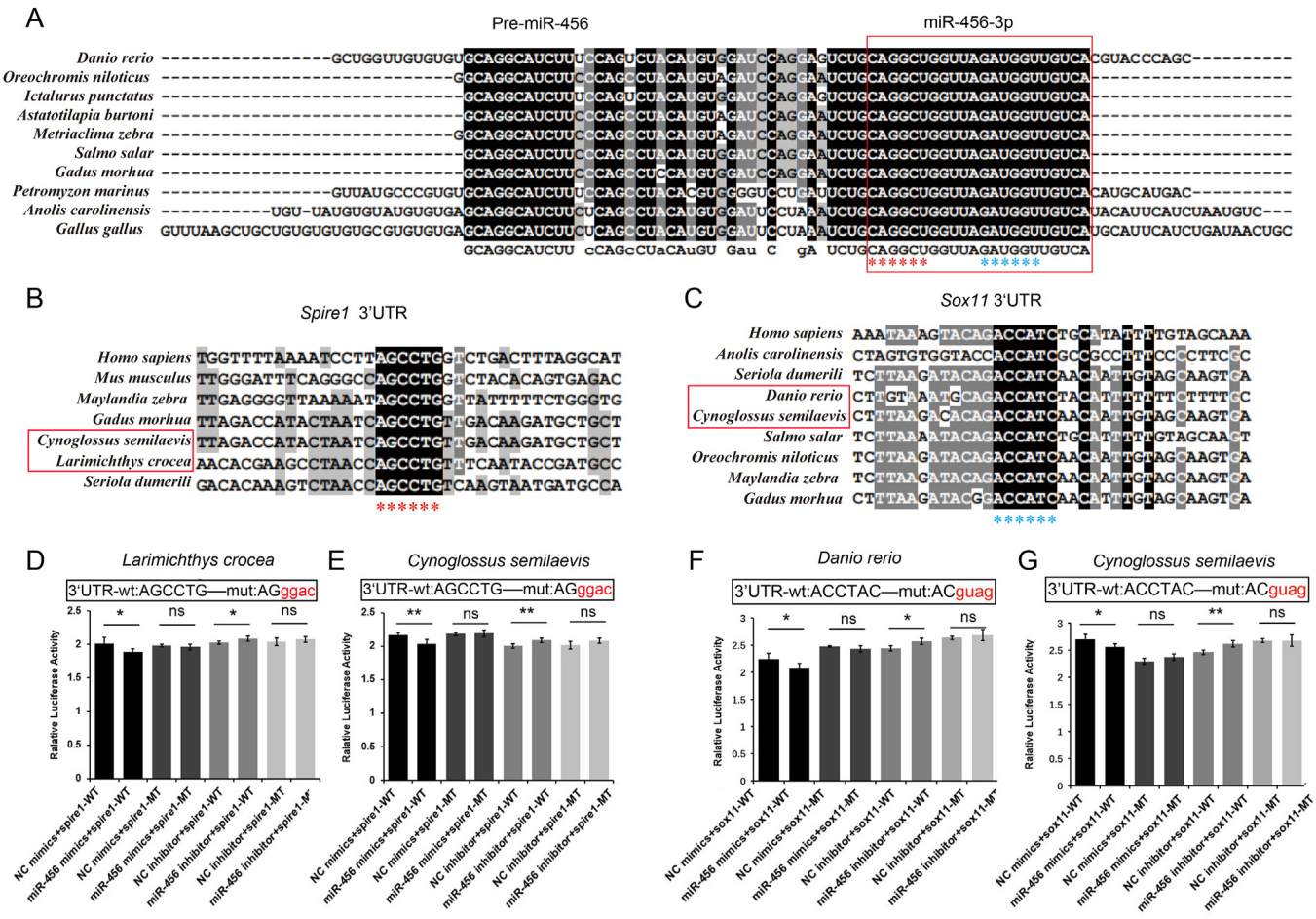

Fig. 9. Conservation of sequence and universality of binding mechanisms in other fish species. (**A**) Sequence alignment of pre-miR-456 from various species. miR-456-3p sequences are shown in the red box. (**B**) Putative miR-456-3p common binding site of 3′UTR of *Spire1* in various species. C. Putative miR-456-3p common binding site of 3′UTR of *Sox11* in various species. D. Luciferase reporter gene constructs of miR-456-3p binding sites in a wild-type *Spire1* 3′UTR (3′UTR-wt) and a mutated form of 3′UTR (3′UTR-mut) in the large yellow croaker (*L. crocea*). HEK293 cells were transfected with NC or miR-456-3p, along with the wild-type of *Spire1* 3′UTR or the mutant-type of *L. crocea*. E. HEK293 cells were transfected with NC and miR-456-3p, along with *Spire1* 3′UTR of the wild-type (3′UTR-wt) and the mutant-type (3′UTR-mut), respectively, of *C. semilaevis*. F. Luciferase reporter gene constructs of miR-456-3p binding sites in a wild type of *Sox11* 3′UTR (3′UTR-wt) and a mutated form of 3′UTR (3′UTR-mut) in zebrafish (*D. rerio*). G. miR-456-3p binding sites in a wild type of *Sox11* 3′UTR (3′UTR-wt) and a mutated form of 3′UTR (3′UTR-mut) of *C. semilaevis*. The luciferase activity was measured and normalized to Renilla luciferase activity. All data represent the mean ± SE. Note: *, $P < 0.05$; **, $P < 0.01$.

distributed in the spermatocyte and spermatozoa (Fig. 5A), whereas the fluorescence signal in the ovary was concentrated in the follicular cavity (Fig. 5B).

3.5. Association of miR-456 with the target genes spire1 and sox11

The target sequence site for miR-456 was the 3′UTR in *spire1* and *sox11* (Fig. 6A). To verify the regulatory effect of miR-456 on *spire1* and *sox11*, wild-type dual luciferase reporter plasmids (*spire1* 3′-UTR WT, *sox11* 3′-UTR WT) and mutant dual luciferase reporter plasmids (*spire1* 3′-UTR MT, *sox11* 3′-UTR MT) were constructed for the 3′-UTR target sites of *spire1* and *sox11*. Theoretically, the co-transfection of miRNAs with 3′-UTR WT of the target genes should inhibit the expression of the WT target gene and ablate the luciferase activity, but not affect the MT target gene that lacks the miRNA interaction region (Fig. 6A). 293 T cells transfected with miR-456+*spire1*-WT group had significantly lower fluorescence than the NC mimics+*spire1*-WT group ($P < 0.01$). The miR-456 mimics+*spire1*-MT had a similar signal to the NC mimics+*spire1*-MT group. The fluorescence of the miR-456 inhibitor+*spire1*-WT group was significantly higher than the NC inhibitor+*spire1*-WT group ($P < 0.05$). The miR-456 inhibitor+*spire1*-MT group was not significantly different from the NC inhibitor + *spire1*-MT group (Fig. 6B). Similarly, the fluorescence of 293 T cells transfected with the miR-456+*sox11*-WT group was significantly lower than the NC mimics+*sox11*-WT group ($P < 0.01$) while miR-456 mimics+*sox11*-MT group was not significantly different from the NC mimics+*sox11*-MT group ($P > 0.01$). The miR-456 inhibitor+*sox11*-WT group was significantly higher than the NC inhibitor+*sox11*-WT group ($P < 0.01$). The miR-456 inhibitor+*sox11*-MT group was not significantly different from the NC inhibitor+*sox11*-MT group ($P > 0.05$) (Fig. 6C).

3.6. Dual-luciferase assay of miR-456 and its ncRNA-targets circklhl29 and ASTR

Bioinformatics analysis identified binding sites for miR-456 at the 3′UTR of the targets *circklhl29* and *ASTR* (Fig. 7A). The interaction between miRNA and targets was determined by constructing and testing wild-type (*circklhl29* 3′-UTR WT, *ASTR* 3′-UTR WT) and mutant (*circklhl29* 3′-UTR MT, *ASTR* 3′-UTR MT) dual-luciferase reporter plasmids (Fig. 7B). We found that 293 T cells transfected with the miR-456+*circklhl29*-WT group had a significantly lower fluorescence than the NC mimics + *circklhl29*-WT group ($P < 0.01$), as well as the miR-456 mimics+*circklhl29*-MT group. The fluorescence value of 293 T cells transfected with the miR-456 inhibitor+*circklhl29*-WT group was

significantly higher than the NC inhibitor+*circklhl29*-WT group,as well as the miR-456 inhibitor+*circklhl29*-MT group ($P < 0.05$) (Fig. 7C). The fluorescence value of 293 T cells transfected with the miR-456+*ASTR*-WT group was significantly lower than the NC mimics+*ASTR*-WT group and the miR-456 mimics+*ASTR*-MT group ($P < 0.05$). The fluorescence value of 293 T cells transfected with the miR-456 inhibitor+*ASTR*-WT group was significantly higher than the NC inhibitor+*ASTR*-WT group and the miR-456 inhibitor+*ASTR*-MT group ($P < 0.01$) (Fig. 7D).

3.7. *In vivo validation of the regulatory effect of miR-456 on the target sox11 and spire1 expression levels through AGO/ANTAGO-miR-456 injection*

The testicular injection of miR-456 agonist in males inhibited the expression levels of the target genes *sox11* and *spire1* relative to the control group. The addition of a miR-456 antagonist upregulated the expression of the target genes *sox11* and *spire1* compared to the control group (Fig. 8A). In the ovaries of females, there were no regulatory effects of agonists and antagonists from the miR-456 injection on the expression of the target genes *sox11* and *spire1* (Fig. 8B).

3.8. *Conservation of the sequence structure of sox11 and spire1 in other fish species*

To investigate the conservation of miR-456-3p and its corresponding target gene binding sites, we first examined the sequence alignment of pre miR-456-3p from different species. From fish to mammals, as expected, mature miR-456-3p is highly conserved (Fig. 9A), and the corresponding binding sites of the two target genes *spire1* and *sox11* still share a common basic sequence with miR-456-3p (Fig. 9B and C). Luciferase reporter gene plasmids were generated based on the *spire1* 3′UTR of *L. crocea* and *C. semilaevis*, as well as the *sox11* 3′UTR of *D. rerio* and *C. semilaevis*. The *spire1/Sox11* 3′UTR were introduced into the pmirGLO vectors along with mutant forms lacking the miR-456 binding site as controls. It was noteworthy that when co-transfected with *spire1* 3′UTR of *L. crocea* and *C. semilaevis,* miR-456-3p mimics were sufficient to reduce luciferase activity, while inhibitors of miR-456-3p enhanced the fluorescence ratio of reporter genes, with no effect on luciferase activity in mutant variants (Fig. 9D and E). Similar results were also obtained when both *D. rerio* and *C. semilaevis* were co-infected with the 3′UTR of *sox11* (Fig. 9F and G). These results indicate that miR-456-3p can also target the *spire1* and *sox11* genes of other bony fish.

4. Discussion

The delayed gonad development and vulnerability to environmental influences in greater amberjack (*Seriola dumerili*) have hindered its stable production in aquaculture (Fakriadis et al., 2019). The histological process of gonadal differentiation, sex steroid hormone changes, and sex-related SNPs have been studied in *S. dumerili* (Papadaki et al., 2021; Kawase et al., 2018), but not the regulatory mechanisms of gonad development at the epigenetic level. Sex-biased ncRNAs are involved in a multi-step process of cell differentiation, including proliferation and differentiation of spermatogonia, meiosis of spermatocytes, and spermiogenesis of sperm cells, which were regulated on the transcription, epigenetic-ncRNA (miRNA, circRNA, lncRNA), and translation levels (Kotaja, 2014; Hu et al., 2018). To go deep into the sex differentiation mechanism of oceanic fish species, taking the greater amberjack as an example, this study analyzed the ncRNA expression patterns in the ovary and testis at the whole transcriptome level and constructed ceRNA networks with sex-biased ncRNAs.

CeRNA interaction networks are efficient epigenetic regulators in the reproductive physiology of multiple species (Tang et al., 2022a). The phased expression of circRNA and its ceRNA regulation were investigated during the testicle development of *Ovis aries*, and the targeting associations in the network between circ_024949 and circ_026259, or IGF1 and oar-miR-29b, were verified (Li et al., 2021). In mice, circRNA9119 could be used as an endogenous sponge to regulate the related ceRNA network by competitively binding miR-26a/miR-136, resulting in up-regulation of TLR 3 and RIG-I in testis somatic cells (Qin et al., 2019). Another ceRNA network, composed of *circdmrt1*, lnc*AMSDT*, cse-miR-196, and *gsdf* (gonadal soma-derived factor), was identified related to sex determination and differentiation in the flatfish half smooth-tongued sole (*C. semilaevis*) (Tang et al., 2022a). Constructing a ceRNA network by sex-biased ncRNAs to regulate reproductive development and sex differentiation has been revealed as a universal epigenetic regulatory mechanism that spans multiple animal groups. In this study, the ceRNA network constructed with sex-biased miR-214, miR-143, and miR-456 as the core has clearly targeted mRNAs or circle/lncRNAs related to sex differentiation regulation. The testis-biased *spire1* and *lncASTR*, working as the targets of miR-456, were involved in the regulation of the male gonadal development process. *Spire1* was the common target of three ncRNAs. MiR-143 increased during follicular growth, and negatively regulated HSD17β4, ER1, and PTGS2 to affect the production of estrogen, androgens, progesterone, and prostaglandins (Zhong et al., 2020). It negatively regulates follicle-stimulating hormone (FSH) production by binding to the 3′-UTR of *KRAS* mRNA instead of a direct interaction with the follicle stimulating hormone receptor gene (*FHSR*) (Zhang et al., 2017). Thus, the regulatory mechanism of miR-143 on the estrogen receptor gene and estrogen production to affect female directional differentiation through the ceRNA network is still unclear and needs further study. MiR-456 had an inhibitory effect on *circklhl29* and *lncASTR* resulting in their upregulation in the testis of *S. dumerili*, with miR-456 downregulated. Meanwhile, *sox11*, *spire1*, and *circtesk1* were overexpressed in the testis compared with the ovary, while *esr1* was ovary-biased, which was consistent with a study that found that *esr1* had the highest expression in the ovary tissues of *Perca flavescens* (Lynn et al., 2007). In *C. semilaevis*, *tesk1* was mainly expressed in the testis and was responsible for spermatogenesis (Meng et al., 2014), while the chromosome Z-linked gene *klhl29* showed a high expression pattern in the male gonad (Wang et al., 2022). The hostgene of *circklhl29* and *circtesk1* (*klhl29* and *tesk1*) also exhibited higher expression in males. To summarize, testis-biased *circklhl29* and *lncASTR* might possess the function of competitive binding to miR-456 and eliminating the endogenous inhibition of miR-456 on the target *spire1*, which means *circklhl29* and *lncASTR* could affect male sexual development through the regulation of the ceRNA network in *S. dumerili*. When miR-456 binds to *circklhl29* or *lncASTR*, the inhibitory effects of miR-456 on *sox11* and *spire1* are released, and their normal expression leads to male development. However, when the sponge effect of ceRNA is released, miR-456 could bind to *sox11* and *spire1* and inhibit their expression, which could result in the gonads developing into females.

The gene *hsd17b1* is related to sex determination in *S. dumerili* (Kawase et al., 2018) and was highly expressed in males in our study. Here we also suggest that *spire1* is involved in the regulation of fish sex differentiation. *Spire1*, named from mutant female sterile *Drosophila* (Manseau and Schüpbach, 1989), can affect the transport process in the intima by regulating actin filament tissue (Welz and Kerkhoff, 2023; Scalzitti et al., 2022; Bosch et al., 2007). Its role in the formation of vesicle-originated actomyosin networks provided functions beyond the cortical actin filament trajectory along microtubule transport and intracellular transport (Alzahofi et al., 2020; Schuh, 2011). Spire-1, Spire-2, and Fmn-2 of the Formin (FMN) subgroup of formin can interact directly and cooperate in the regulation of actin structures (Dietrich et al., 2013; Montaville et al., 2014, 2016), and spermatogenesis (Wang et al., 2020). *Spire1* and *spire2* were highly expressed in mouse oocytes and were key factors in their asymmetric division (Pfender et al., 2011). *Rab11a* attracted the actin nucleation factors *spire1* and *Formin-2* to the fertilization cone, where they locally nucleate actin and further accelerate prokaryotic migration (Scheffler et al., 2021). *Spire1* and *spire2* were also highly expressed in the testis of adult rats; knockdown of *spire1* in the testis affected the F-actin network and hindered the adhesion function of

sperm cells, thereby causing premature sperm shedding from the spermatogenic epithelium and interfering with the transport of sperm cells across the epithelium (Wen et al., 2018). In this study, we determined that *spire1* existed in the sex differential ceRNA networks and might play a functional role in dynamic transport during spermatogenesis, which is worth exploring further. Our study also demonstrated, through a sequence comparison and experimentation, a cross-species conservative model of the mechanism by which miRNAs and target genes bind through specific binding site in bony fish, a mechanism that has long been widely discussed and has been verified to varying degrees in multiple species (Liu et al., 2018; Wang et al., 2024).

The direct binding of miR-456 to *sox11* can be used as a post-transcriptional co-regulator to maintain the undifferentiated state of the chicken blastoderm and regulate pluripotency in chicken embryo disc cells and primordial germ cells by silencing somatic gene expression (Lee et al., 2011). Our results suggested that the Wnt signaling pathway might be one of the critical ways for ncRNAs to regulate the sexual differentiation of *S. dumerili*. *WNT4* plays an important role in sex determination and gonadal development in multiple species (McClatchey et al., 1992). In mice, *WNT4* affected ovarian development, participating in the formation of the Mullerian duct (Stark et al., 1994). In humans, *WNT4* and *DAX1* collaborated to regulate female ovarian development and prevent testicular formation (Jordan et al., 2001). In black snapper (*Apsilus dentatus*), *WNT4* participated in the regulation of early ovarian development, growth, and maturation (Wu and Chang, 2009). In Japanese flounder(*Paralichthys olivaceus*), *WNT4* was expressed in both the ovary and testis, but was ovary-biased (Weng, 2013). The *Sox* family has emerged as modulators of canonical Wnt/β-catenin signaling in diverse development and disease contexts. For instance, *sox11* can directly repress Wnt/β-Catenin signaling (Peiyu, 2012) and can be induced via Wnt7b (Yu et al., 2020), indicating noteworthy interactions occur between *sox* and *wnt* families. The Wnt signaling pathway also connects to actin cytoskeleton remodeling, and there is mutual communication between actin and microtubule cytoskeletons. The activation of the non-classical Wnt signaling pathway is related to the transfer of microtubule-dependent androgen receptors (Miyamoto et al., 2015). This implicates potential crosstalk between Wnt and *spire1*. Thus, the ceRNA networks constructed in this study could help to figure out a clearer sex differentiation mechanism in fish. We predict that members of the ceRNA network, especially ncRNAs and their agonists/antagonists, will have broad applications in regulating fish gonadal differentiation.

5. Conclusion

This study revealed that sex-biased ncRNAs participated in the mechanism of gonad development through interacting with sex-related genes including *spire1* and *sox1*1 by forming a ceRNA regulatory network in *S. dumerili*. Female-biased miR-456 targeted *spire1* and *sox11*, while male-biased *circklhl29* and *ASTR* acted as sponges of miR-456 and upregulated the expression of *spire1* and *sox11*. In summary, *circklhl29*, *ASTR*, miRNA-456, and *spire1/sox11* constructed a ceRNA regulatory network that probably affects the sex differentiation process of *S. dumerili*, providing a theoretical basis for the sex differentiation regulation by ncRNAs in fish.

CRediT authorship contribution statement

Na Zhao: Writing – original draft, Validation, Resources, Methodology, Investigation, Funding acquisition, Formal analysis. **Xiaoxu He:** Writing – original draft, Visualization, Validation. **Qianwen Min:** Software. **Deborah Mary Power:** Writing – review & editing. **Zhongdian Dong:** Supervision. **Changgeng Yang:** Supervision. **Bo Zhang:** Writing – review & editing, Supervision, Project administration, Conceptualization.

Ethical Statement

All animal experiments followed the guidelines and were approved by the Animal Research and Ethics Committee of the Institute of Aquatic Economic Animals, Guangdong Ocean University (ZJW20221102056).

Funding

This research was financed by the Fund of Southern Marine Science and EngineeringGuangdong Laboratory (Zhanjiang) (ZJW-2023-01), the Guangdong Basic and Applied Basic Research Foundation (2023A1515010576; 20241515012859), the Youth Science and Technology Innovation Project in 2024 (2023E0006).

Declaration of competing interest

The authors declare no competing interests.

Acknowledgments

We thanked Professor CH Zhu for his assistance in obtaining tissue samples from the fish.

Appendix A. Supplementary data

Supplementary data to this article can be found online at https://doi.org/10.1016/j.watbs.2025.100370.

References

Alzahofi, N., Welz, T., Robinson, C.L., et al., 2020. Rab27a co-ordinates actin-dependent transport by controlling organelle-associated motors and track assembly proteins. Nat. Commun. 11 (1), 3495. https://doi.org/10.1038/s41467-020-17212-6.

Betel, D., Wilson, M., Gabow, A., et al., 2008. The microRNA. org resource: targets and expression. Nucleic Acids Res. 36 (Suppl. 1), D149–D153. https://doi.org/10.1093/nar/gkm995.

Bosch, M., Le, K.H., Bugyi, B., et al., 2007. Analysis of the function of Spire in actin assembly and its synergy with formin and profilin. Mol. Cell 28 (4), 555–568. https://doi.org/10.1016/j.molcel.2007.09.018.

Brown, M.S., Evans, B.S., Afonso, L.O.B., 2020. Discordance for genotypic sex in phenotypic female Atlantic salmon (*Salmo salar*) is related to a reduced sdY copy number. Sci. Rep. 10 (1), 9651. https://doi.org/10.1038/s41598-020-66406-x.

Chakraborty, T., Zhou, L.Y., Chaudhari, A., et al., 2016. Dmy initiates masculinity by altering Gsdf/Sox9a2/Rspo1 expression in medaka (*Oryzias latipes*). Sci. Rep. 6, 19480. https://doi.org/10.1038/srep19480.

Corriero, A., Wylie, M.J., Nyuji, M., et al., 2021. Reproduction of greater amberjack (*Seriola dumerili*) and other members of the family carangidae. Rev. Aquacult. 13 (4), 1781–1815.

Cui, Z., Liu, Y., Wang, W., et al., 2017. Genome editing reveals dmrt1 as an essential male sex-determining gene in the Chinese tongue sole (*Cynoglossus semilaevis*). Sci. Rep. 7, 42213. https://doi.org/10.1038/srep42213.

Deng, Q., Zhao, N., Zhu, C., et al., 2022. Long non-coding RNAs in the physiology of aquaculture animals: a perspective update. Rev. Fish Biol. Fish. 1–20. https://doi.org/10.1007/s11160-022-09734-7.

Deng, Q., Zhao, N., Ru, X., et al., 2023. Sex-inclined piwi-interacting RNAs in serum exosomes for sex determination in the greater amberjack (*Seriola dumerili*). Int. J. Mol. Sci. 24 (4), 3438. https://doi.org/10.3390/ijms24043438. Published 2023 Feb 8.

Dietrich, S., Weiß, S., Pleiser, S., et al., 2013. Structural and functional insights into the Spir/formin actin nucleator complex. Biol. Chem. 394 (12), 1649–1660. https://doi.org/10.1515/hsz-2013-0176.

Dong, Y., Lyu, L., Zhang, D., et al., 2021. Integrated lncRNA and mRNA transcriptome analyses in the ovary of *Cynoglossus semilaevis* reveal genes and pathways potentially involved in reproduction. Front. Genet. 12, 671729. https://doi.org/10.3389/fgene.2021.671729.

Duan, W., Gao, F.X., Chen, Z.W., et al., 2021. A sex-linked SNP mutation in amhr2 is responsible for male differentiation in obscure puffer (*Takifugu obscurus*). Mol. Biol. Rep. 48 (8), 6035–6046. https://doi.org/10.1007/s11033-021-06606-4.

Enright, A.J., John, B., Gaul, U., et al., 2003. MicroRNA targets in Drosophila. Genome Biol. 5 (1), R1. https://doi.org/10.1186/gb-2003-5-1-r1.

Fakriadis, I., Lisi, F., Sigelaki, I., et al., 2019. Spawning kinetics and egg/larval quality of greater amberjack (*Seriola dumerili*) in response to multiple GnRHa injections or implants. Gen. Comp. Endocrinol. 279, 78–87. https://doi.org/10.1016/j.ygcen.2018.12.007.

Fakriadis, I., Sigelaki, I., Papadaki, M., et al., 2020. Control of reproduction of greater amberjack *Seriola dumerili* reared in aquaculture facilities. Aquaculture 519, 519.

Feng, B., Li, S., Wang, Q., et al., 2021. lncRNA DMRT2-AS acts as a transcriptional regulator of dmrt2 involving in sex differentiation in the Chinese tongue sole (*Cynoglossus semilaevis*). Comparative biochemistry and physiology. Part B, Biochemistry & molecular biology 253, 110542. https://doi.org/10.1016/j.cbpb.2020.110542.

Friedlander, M.R., Mackowiak, S.D., Li, N., et al., 2012. miRDeep2 accurately identifies known and hundreds of novel microRNA genes in seven animal clades. Nucleic Acids Res. 40 (1), 37–52. https://doi.org/10.1093/nar/gkr688.

Gao, Y., Wang, J., Zhao, F., 2015. CIRI: an efficient and unbiased algorithm for de novo circular RNA identification. Genome Biol. 16 (1), 4. https://doi.org/10.1186/s13059-014-0571-3.

Griffiths-Jones, S., Grocock, R.J., van Dongen, S., et al., 2006. miRBase: microRNA sequences, targets and gene nomenclature. Nucleic Acids Res. 34 (Database issue), D140–D144. https://doi.org/10.1093/nar/gkj112.

He, Z., Ma, Z., Yang, D., et al., 2022. Circular RNA expression profiles and CircSnd1-miR-135b/c-foxl2 axis analysis in gonadal differentiation of protogynous hermaphroditic ricefield eel *Monopterus albus*. BMC Genom. 23 (1), 552. https://doi.org/10.1186/s12864-022-08783-3.

Hou, M., Wang, Q., Zhang, J., et al., 2023. Differential expression of miRNAs, lncRNAs, and circRNAs between ovaries and testes in common carp (*Cyprinus carpio*). Cells 12 (22), 2631. https://doi.org/10.3390/cells12222631.

Hu, J., Sun, F., Handel, M.A., 2018. Nuclear localization of EIF4G3 suggests a role for the XY body in translational regulation during spermatogenesis in mice. Biol. Reprod. 98 (1), 102–114. https://doi.org/10.1093/biolre/iox150.

Huang, T., Gu, W., Liu, E., et al., 2021. Comprehensive analysis of miRNA-mRNA/lncRNA during gonadal development of triploid female rainbow trout (*Oncorhynchus mykiss*). Genomics 113 (6), 3533–3543. https://doi.org/10.1016/j.ygeno.2021.08.018.

Jia, J.Y., Chen, G.H., Shu, T.T., et al., 2024. Androgen signaling inhibits de novo lipogenesis to alleviate lipid deposition in zebrafish. Zool. Res. 45 (2), 355–366. https://doi.org/10.24272/j.issn.2095-8137.2023.324.

Jiang, D.N., Yang, H.H., Li, M.H., et al., 2016. Gsdf is a downstream gene of dmrt1 that functions in the male sex determination pathway of the Nile tilapia. Mol. Reprod. Dev. 83 (6), 497–508. https://doi.org/10.1002/mrd.22642.

Jordan, B.K., Mohammed, M., Ching, S.T., et al., 2001. Up-regulation of WNT-4 signaling and dosage-sensitive sex reversal in humans. Am. J. Hum. Genet. 68 (5), 1102–1109. https://doi.org/10.1086/320125.

Karreth, F.A., Reschke, M., Ruocco, A., et al., 2015. The BRAF pseudogene functions as a competitive endogenous RNA and induces lymphoma in vivo. Cell 161 (2), 319–332. https://doi.org/10.1016/j.cell.2015.02.043.

Kawase, J., Aoki, J.Y., Hamada, K., et al., 2018. Identification of sex-associated SNPs of greater amberjack (*Seriola dumerili*). Journal of genomics 6, 53–62. https://doi.org/10.7150/jgen.24788.

Kim, D., Paggi, J.M., Park, C., et al., 2019. Graph-based genome alignment and genotyping with HISAT2 and HISAT-genotype. Nat. Biotechnol. 37 (8), 907–915. https://doi.org/10.1038/s41587-019-0201-4.

Kotaja, N., 2014. MicroRNAs and spermatogenesis. Fertil. Steril. 101, 1552–1562. https://doi.org/10.1016/j.fertnstert.2014.04.025.

Langmead, B., Trapnell, C., Pop, M., et al., 2009. Ultrafast and memory-efficient alignment of short DNA sequences to the human genome. Genome Biol. 10, R25. https://doi.org/10.1186/gb-2009-10-3-r25.

Lee, S.I., Lee, B.R., Hwang, Y.S., et al., 2011. MicroRNA-mediated posttranscriptional regulation is required for maintaining undifferentiated properties of blastoderm and primordial germ cells in chickens. Proc. Natl. Acad. Sci. U.S.A. 108 (26), 10426–10431. https://doi.org/10.1073/pnas.1106141108.

Lewis, B.P., Shih, I.H., Jonesrhoades, M.W., et al., 2003. Prediction of mammalian microRNA targets. Cell 115 (7), 787–798. https://doi.org/10.1016/s0092-8674(03)01018-3.

Li, M., Sun, Y., Zhao, J., 2015. A tandem duplicate of anti-müllerian hormone with a missense SNP on the Y chromosome is essential for male sex determination in nile Tilapia, *Oreochromis niloticus*. PLoS Genet. 11 (11), e1005678. https://doi.org/10.1371/journal.pgen.1005678.

Li, T., Luo, R., Wang, X., et al., 2021. Unraveling stage-dependent expression patterns of circular RNAs and their related ceRNA modulation in ovine postnatal testis development. Front. Cell Dev. Biol. 9, 627439. https://doi.org/10.3389/fcell.2021.627439.

Li, Y., Li, X., Ye, D., et al., 2024. Endogenous biosynthesis of docosahexaenoic acid (DHA) regulates fish oocyte maturation by promoting pregnenolone production. Zool. Res. 45 (1), 176–188. https://doi.org/10.24272/j.issn.2095-8137.2023.032.

Liu, L., Zhu, W., Liu, J., et al., 2018. Identification and differential regulation of microRNAs during thyroid hormone-dependent metamorphosis in Microhyla fissipes. BMC Genom. 19 (1), 507. https://doi.org/10.1186/s12864-018-4848-x.

Livak, K.J., Schmittgen, T.D., 2001. Analysis of relative gene expression data using real-time quantitative PCR and the 2(-Delta Delta C(T)) Method. Methods (San Diego, Calif.) 25 (4), 402–408. https://doi.org/10.1006/meth.2001.1262.

Ma, Z., Yang, J., Zhang, Q., et al., 2021. miR-133b targets tagln2 and functions in tilapia oogenesis. Comparative biochemistry and physiology. Part B. Biochemistry & molecular biology 256, 110637. https://doi.org/10.1016/j.cbpb.2021.110637.

Manseau, L.J., Schüpbach, T., 1989. Cappuccino and spire: two unique maternal-effect loci required for both the anteroposterior and dorsoventral patterns of the Drosophila embryo. Gene Dev. 3 (9), 1437–1452. https://doi.org/10.1101/gad.3.9.1437.

McClatchey, A.I., Van den Bergh, P., Pericak-Vance, M.A., et al., 1992. Temperature-sensitive mutations in the III-IV cytoplasmic loop region of the skeletal muscle sodium channel gene in paramyotonia congenita. Cell 68 (4), 769–774. https://doi.org/10.1016/0092-8674(92)90151-2.

Memczak, S., Jens, M., Elefsinioti, A., et al., 2013. Circular RNAs are a large class of animal RNAs with regulatory potency. Nature 495 (7441), 333–338. https://doi.org/10.1038/nature11928.

Meng, L., Zhu, Y., Zhang, N., et al., 2014. Cloning and characterization of tesk1, a novel spermatogenesis-related gene, in the tongue sole (*Cynoglossus semilaevis*). PLoS One 9 (10), e107922. https://doi.org/10.1371/journal.pone.0107922.

Miyamoto, D.T., Zheng, Y., Wittner, B.S., et al., 2015. RNA-Seq of single prostate CTCs implicates noncanonical Wnt signaling in antiandrogen resistance. Science (New York, N.Y.) 349 (6254), 1351–1356. https://doi.org/10.1126/science.aab0917.

Montaville, P., Jégou, A., Pernier, J., et al., 2014. Spire and Formin 2 synergize and antagonize in regulating actin assembly in meiosis by a ping-pong mechanism. PLoS Biol. 12 (2), e1001795. https://doi.org/10.1371/journal.pbio.1001795.

Montaville, P., Kühn, S., Compper, C., et al., 2016. Role of the C-terminal extension of formin 2 in its activation by spire protein and processive assembly of actin filaments. J. Biol. Chem. 291 (7), 3302–3318. https://doi.org/10.1074/jbc.M115.681379.

Ning, X.H., Han, B., Peng, Y., et al., 2024. LncRNA pol-lnc78 as a ceRNA regulates antibacterial responses via suppression of pol-miR-n199-3p-mediated SARM down-regulation in *Paralichthys olivaceus*. Zool. Res. 45 (1), 25–35. https://doi.org/10.24272/j.issn.2095-8137.2022.520.

Papadaki, M., Mandalakis, M., Anastasiou, T.I., et al., 2021. Histological evaluation of sex differentiation and early sex identification in hatchery-produced greater amberjack (*Seriola dumerili*) reared in sea cages. Fish Physiol. Biochem. 47 (6), 1777–1792. https://doi.org/10.1007/s10695-021-01007-7.

Peiyu, Kuo M., 2012. Sox11 directly represses wnt/β-catenin signaling and identifies a subgroup of mantle cell lymphoma patients with improved survival with intensive treatment. Blood 120 (21), 895. https://doi.org/10.1182/blood.V120.21.895.895.

Perez, J.A., Papadakis, I.E., Papandroulakis, N.C., et al., 2020. The ontogeny of greater amberjack digestive and antioxidant defence systems under different rearing conditions: a histological and enzymatic approach. Aquacult. Nutr. 26 (6).

Pertea, M., Kim, D., Pertea, G.M., et al., 2016. Transcript-level expression analysis of RNA-seq experiments with HISAT, StringTie and Ballgown. Nat. Protoc. 11 (9), 1650–1667. https://doi.org/10.1038/nprot.2016.095.

Pfender, S., Kuznetsov, V., Pleiser, S., et al., 2011. Spire-type actin nucleators cooperate with Formin-2 to drive asymmetric oocyte division. Curr. Biol.: Cailiao Baohu 21 (11), 955–960. https://doi.org/10.1016/j.cub.2011.04.029.

Qin, L., Lin, J., Xie, X., 2019. CircRNA-9119 suppresses poly I:C induced inflammation in Leydig and Sertoli cells via TLR3 and RIG-I signal pathways. Mol. Med. 25, 28. https://doi.org/10.1186/s10020-019-0094-1.

Rehmsmeier, M., Steffen, P., Hochsmann, M., et al., 2004. Fast and effective prediction of microRNA/target duplexes. RNA (New York, N.Y.) 10 (10), 1507–1517. https://doi.org/10.1261/rna.5248604.

Rui, X.J., Nan, H., Yu, W.D., et al., 2024. Potential therapeutic role of spermine via Rac1 in osteoporosis: insights from zebrafish and mice. Zool. Res. 45 (2), 367–380. https://doi.org/10.24272/j.issn.2095-8137.2023.371.

Sarropoulou, E., Sundaram, A.Y.M., Kaitetzidou, E., et al., 2017. Full genome survey and dynamics of gene expression in the greater amberjack *Seriola dumerili*. GigaScience 6 (12), 1–13. https://doi.org/10.1093/gigascience/gix108.

Scalzitti, S., Mariani, D., Setti, A., et al., 2022. Lnc-SMaRT translational regulation of Spire1, A new player in muscle differentiation. J. Mol. Biol. 434 (2), 167384. https://doi.org/10.1016/j.jmb.2021.167384.

Scheffler, K., Uraji, J., Jentoft, I., et al., 2021. Two mechanisms drive pronuclear migration in mouse zygotes. Nat. Commun. 12 (1), 841. https://doi.org/10.1038/s41467-021-21020-x.

Schuh, M., 2011. An actin-dependent mechanism for long-range vesicle transport. Nat. Cell Biol. 13 (12), 1431–1436. https://doi.org/10.1038/ncb2353.

Shannon, P., Markiel, A., Ozier, O., et al., 2003. Cytoscape: a software environment for integrated models of biomolecular interaction networks. Genome Res. 13 (11), 2498–2504. https://doi.org/10.1101/gr.1239303.

Stark, K., Vainio, S., Vassileva, G., et al., 1994. Epithelial transformation of metanephric mesenchyme in the developing kidney regulated by Wnt-4. Nature 372 (6507), 679–683. https://doi.org/10.1038/372679a0.

Tang, R., Xu, C., Zhu, Y., et al., 2022. Identification and expression analysis of sex biased miRNAs in Chinese hook snout carp *Opsariichthys bidens*. Front. Genet. 13, 990683. https://doi.org/10.3389/fgene.2022.990683.

Tang, L., Huang, F., You, W., et al., 2022a. ceRNA crosstalk mediated by ncRNAs is a novel regulatory mechanism in fish sex determination and differentiation. Genome Res. 32 (8), 1502–1515. https://doi.org/10.1101/gr.275962.121.

Wang, S.H., Ma, F., Tang, Z.H., et al., 2016. Long non-coding RNA H19 regulates FOXM1 expression by competitively binding endogenous miR-342-3p in gallbladder cancer. J. Exp. Clin. Cancer Res.: CR 35 (1), 160. https://doi.org/10.1186/s13046-016-0436-6.

Wang, L., Yan, M., Wu, S., et al., 2020. Actin binding proteins, actin cytoskeleton and spermatogenesis - lesson from toxicant models. Reprod. Toxicol. 96, 76–89. https://doi.org/10.1016/j.reprotox.2020.05.017.

Wang, N., Gao, J., Liu, Y., et al., 2022. Identification of crucial factors involved in *Cynoglossus semilaevis* sexual size dimorphism by GWAS and demonstration of zbed1 regulatory network by DAP-seq. Genomics 114 (3), 110376. https://doi.org/10.1016/j.ygeno.2022.110376.

Wang, Y., Tang, X., Lu, J., 2024. Convergent and divergent evolution of microRNA-mediated regulation in metazoans. Biol. Rev. Camb. Phil. Soc. 99 (2), 525–545. https://doi.org/10.1111/brv.13033.

Welz, T., Kerkhoff, E., 2023. The role of SPIRE actin nucleators in cellular transport processes. J. Cell Sci. 136 (6), jcs260743. https://doi.org/10.1242/jcs.260743.

Wen, Q., Li, N., Xiao, X., et al., 2018. Actin nucleator Spire 1 is a regulator of ectoplasmic specialization in the testis. Cell Death Dis. 9 (2), 208. https://doi.org/10.1038/s41419-017-0201-6.

Weng, S.D., 2013. Cloning and RT-PCR Differential Expression Profile Analysis of Sex-Related Genes in Paralichthysolivaceus [D]. Graduate School of Chinese Academy of Sciences (Institute of Oceanography).

Wu, G.C., Chang, C.F., 2009. wnt4 Is associated with the development of ovarian tissue in the protandrous black Porgy, *Acanthopagrus schlegeli*. Biol. Reprod. 81 (6), 1073–1082. https://doi.org/10.1095/biolreprod.109.077362.

Yan, H., Shen, X., Cui, X., et al., 2018. Identification of genes involved in gonadal sex differentiation and the dimorphic expression pattern in *Takifugu rubripes* gonad at the early stage of sex differentiation. Fish Physiol. Biochem. 44 (5), 1275–1290. https://doi.org/10.1007/s10695-018-0519-8.

Yu, F., Lu, Z., Cai, J., et al., 2015. MALAT1 functions as a competing endogenous RNA to mediate Rac1 expression by sequestering miR-101b in liver fibrosis. Cell Cycle 14 (24), 3885–3896. https://doi.org/10.1080/15384101.2015.1120917.

Yu, F., Wu, F., Li, F., et al., 2020. Wnt7b-induced Sox11 functions enhance self-renewal and osteogenic commitment of bone marrow mesenchymal stem cells. Stem Cell. 38 (8), 1020–1033. https://doi.org/10.1002/stem.3192.

Yu, Q., Peng, C., Ye, Z., et al., 2020. An estradiol-17β/miRNA-26a/cyp19a1a regulatory feedback loop in the protogynous hermaphroditic fish, *Epinephelus coioides*. Mol. Cell. Endocrinol. 504, 110689. https://doi.org/10.1016/j.mce.2019.110689.

Zhang, L., Zhang, X., Zhang, X., et al., 2017. MiRNA-143 mediates the proliferative signaling pathway of FSH and regulates estradiol production. J. Endocrinol. 234 (1), 1–14. https://doi.org/10.1530/JOE-16-0488.

Zhang, B., Zhao, N., Jia, L., et al., 2019. Seminal plasma exosomes: promising biomarkers for identification of male and pseudo-males in *Cynoglossus semilaevis*. Mar. Biotechnol. 21 (3), 310–319. https://doi.org/10.1007/s10126-019-09881-2.

Zhang, B., Zhao, N., Jia, L., et al., 2020. Identification and application of piwi-interacting RNAs from seminal plasma exosomes in *Cynoglossus semilaevis*. BMC Genom. 21 (1), 302. https://doi.org/10.1186/s12864-020-6660-7.

Zhang, X., Zhou, J., Li, L., et al., 2020. Full-length transcriptome sequencing and comparative transcriptomic analysis to uncover genes involved in early gametogenesis in the gonads of Amur sturgeon (*Acipenser schrenckii*). Front. Zool. 17, 11. https://doi.org/10.1186/s12983-020-00355-z.

Zhao, N., Wang, Q., Deng, Q.X., et al., 2023. Heterogeneity of sex-biased miRNAs profiling of *Cynoglossus semilaevis* between exosome and sperm. Aquaculture 563 (1), 738898. https://doi.org/10.1016/j.aquaculture.2022.738898.

Zhong, Y., Li, L., Chen, Z., et al., 2020. MIR143 inhibits steroidogenesis and induces apoptosis repressed by H3K27me3 in granulosa cells. Front. Cell Dev. Biol. 8, 565261. https://doi.org/10.3389/fcell.2020.565261.

Zhong, H., Guo, Z., Xiao, J., et al., 2022. Comprehensive characterization of circular RNAs in ovary and testis from nile Tilapia. Front. Vet. Sci. 9, 847681. https://doi.org/10.3389/fvets.2022.847681.

Zupa, R., Rodríguez, C., Mylonas, C.C., et al., 2017. Comparative study of reproductive development in wild and captive-reared greater amberjack *Seriola dumerili* (risso, 1810). PLoS One 12 (1), e0169645. https://doi.org/10.1371/journal.pone.0169645.